



Naafs, B. D. A., Castro, J. M., de Gea, G. A., Quijano, M. L. L., Schmidt, D. N., & Pancost, R. D. (2016). Gradual and sustained carbon dioxide release during Aptian Oceanic Anoxic Event 1a. *Nature Geoscience*, 9(2), 135-139. DOI: 10.1038/ngeo2627

Peer reviewed version

Link to published version (if available):  
[10.1038/ngeo2627](https://doi.org/10.1038/ngeo2627)

[Link to publication record in Explore Bristol Research](#)  
PDF-document

## **University of Bristol - Explore Bristol Research**

### **General rights**

This document is made available in accordance with publisher policies. Please cite only the published version using the reference above. Full terms of use are available:  
<http://www.bristol.ac.uk/pure/about/ebr-terms.html>

1 **Gradual and sustained carbon dioxide release during Aptian Oceanic Anoxic**  
2 **Event 1a**

3

4 B.D.A. Naafs<sup>1\*</sup>, J.M. Castro<sup>2</sup>, G.A. De Gea<sup>2</sup>, M.L. Quijano<sup>3</sup>, D.N. Schmidt<sup>4</sup>, and R.D.  
5 Pancost<sup>1</sup>

6

7 <sup>1</sup>Organic Geochemistry Unit, School of Chemistry and Cabot Institute, University of  
8 Bristol, BS8 1TS, UK

9 <sup>2</sup>Dept. Geología, CEACTierra, University of Jaén, E-23071, Spain

10 <sup>3</sup>Dept. Química Inorgánica y Orgánica, CEACTierra, University of Jaén, E-23071,  
11 Spain

12 <sup>4</sup>School of Earth Sciences and Cabot Institute, University of Bristol, BS8 1RJ, UK

13

14 \*Corresponding author. Tel. +44-(0)117-9546395. E-mail address:

15 [david.naafs@bristol.ac.uk](mailto:david.naafs@bristol.ac.uk)

16

17 **During the Aptian Oceanic Anoxic Event 1a, about 120 million years ago, black**  
18 **shales were deposited in all the major ocean basins<sup>1</sup>. The event was also**  
19 **associated with elevated sea surface temperatures<sup>2,3</sup> and a calcification crisis in**  
20 **calcareous nannoplankton<sup>4</sup>. These environmental changes have been attributed**  
21 **to variations in atmospheric CO<sub>2</sub> concentrations<sup>2,3,5,6</sup>, but the evolution of the**  
22 **carbon cycle during this event is poorly constrained. Here we present records of**  
23 **atmospheric CO<sub>2</sub> concentrations across Ocean Anoxic Event 1a derived from**  
24 **bulk and compound specific  $\delta^{13}\text{C}$  from marine rock outcrops in southern Spain**  
25 **and Tunisia. We find that CO<sub>2</sub> concentrations doubled in two steps during the**

26 ocean anoxic event and remained above background values for approximately  
27 1.5 to 2 million years before declining. The rise of CO<sub>2</sub> concentrations occurred  
28 over several tens to hundreds of thousand years, and thus was unlikely to have  
29 resulted in any prolonged surface ocean acidification, suggesting that CO<sub>2</sub>  
30 emissions were not the primary cause of the nannoplankton calcification crisis.  
31 We find that the period of elevated CO<sub>2</sub> concentrations coincides with a shift in  
32 the oceanic osmium-isotope inventory<sup>7</sup> associated with emplacement of the  
33 Ontong Java Plateau flood basalts, and conclude that sustained volcanic  
34 outgassing was the primary source of carbon dioxide during Ocean Anoxic Event  
35 1a.

36

37 Oceanic Anoxic Events (OAEs) represent dramatic changes in the climatic and  
38 palaeoceanographic state of the planet. Of these, OAE 1a during the Aptian Stage of  
39 the Early Cretaceous is one of the largest with black shale deposition in all major  
40 ocean basins<sup>1</sup>. Multi-proxy sea surface temperature (SST) estimates from the boreal  
41 realm and Pacific Ocean suggest that OAE 1a was accompanied by a ~ 4-8 °C  
42 increase in SSTs, assumed to be driven by an increase in  $p\text{CO}_2$ <sup>2,3</sup>. In addition, OAE 1a  
43 is concomitant with the calcification crisis of the nannoconids, the most ubiquitous  
44 planktic calcifiers during the Early Cretaceous<sup>4</sup>. Their near disappearance is one of  
45 the most significant events in the nannoplankton fossil record<sup>8</sup>. Their demise as well  
46 as malformation and secretion of dwarfed coccoliths and a reduction in pelagic  
47 carbonate fluxes have been suggested to represent a (calcification) response to  
48 widespread surface ocean acidification due to an increase in  $p\text{CO}_2$ <sup>5</sup>. However the  
49 source of excess CO<sub>2</sub>, potentially methane release from gas hydrates and/or CO<sub>2</sub> from  
50 (submarine) volcanic outgassing, the evolution of  $p\text{CO}_2$  across OAE 1a, and whether

51 this change in  $p\text{CO}_2$  is the driving factor for the calcification crisis remains  
52 controversial<sup>5-7,9-12</sup>. Most importantly, paleo- $p\text{CO}_2$  proxies have yet to confirm  
53 whether changes in  $p\text{CO}_2$  are indeed associated with these biological and  
54 environmental perturbations across OAE 1a and weather surface ocean acidification,  
55 defined here as a coupled decline in (surface) ocean pH and  $\Omega^{13}$  due to rapid input of  
56 carbon into the earth system, has happened at all. Determining the relative timing of  
57 events is crucial in identifying causal relationships and can provide crucial constraints  
58 for the source of  $p\text{CO}_2$ , but has been challenging as most records originate from slow  
59 accumulating deep-sea sediments.

60 To accurately determine the relative timing, we provide a high-resolution  
61 record of  $p\text{CO}_2$  across OAE 1a from an expanded section in Southern Spain (Cau, Fig.  
62 1). OAE 1a is defined as the interval covering segments C3-C6 and has a thickness of  
63 ~ 40 m at Cau, resulting in average sedimentation rate of 2.5 – 4 cm/ka, assuming an  
64 duration of 1-1.3 Myr<sup>14,15</sup>. These sedimentation rates are one order of magnitude  
65 higher than those at the OAE 1a reference section at Cismon, but similar to those at  
66 other expanded OAE 1a sections<sup>16,17</sup>. The hemipelagic sediments consisting of marls,  
67 marly limestones, and black marls (Fig. 2) that contain a rich and well-preserved  
68 fossil association, allowing for a detailed integrated bio- and chemostratigraphy<sup>18,19</sup>.  
69 Importantly, the organic matter at Cau is predominantly of marine origin and  
70 thermally immature<sup>20</sup>. The nannoconid crisis occurs around 42.5 m in the  
71 *Globigerinelloides blowi* planktonic foraminifera zone just before the beginning of the  
72 C3 segment and NCIE<sup>18,19</sup>, identical to other sections<sup>4,16</sup>.

73 To reconstruct changes in  $p\text{CO}_2$  we use paired bulk carbonate ( $\delta^{13}\text{C}_{\text{carb}}$ ) and  
74 organic carbon stable carbon isotopes (either bulk organic,  $\delta^{13}\text{C}_{\text{TOC}}$ , or based on algal  
75 derived lipids such as pristane,  $\delta^{13}\text{C}_{\text{alg}}$ ). The difference between these two records,

76  $\Delta^{13}\text{C}$  (for example,  $\Delta^{13}\text{C}_{\text{bulk}} = \delta^{13}\text{C}_{\text{carb}} - \delta^{13}\text{C}_{\text{TOC}}$ ), can be used to reconstruct changes  
77 in atmospheric  $\text{CO}_2$ <sup>21</sup> and has been applied to reconstruct changes in atmospheric  
78  $p\text{CO}_2$  throughout Earth's history, including the OAEs<sup>22</sup>. The method relies on the  
79 understanding that high  $p\text{CO}_2$ , and hence dissolved  $\text{CO}_2$  concentrations in the surface  
80 ocean, cause greater discrimination against  $^{13}\text{C}$  during algal photosynthesis, leading to  
81 more depleted  $\delta^{13}\text{C}$  values for marine organic matter ( $\delta^{13}\text{C}_{\text{TOC}}$  and  $\delta^{13}\text{C}_{\text{alg}}$ ) compared  
82 to carbonates ( $\delta^{13}\text{C}_{\text{carb}}$ ). Here, we generate a high-resolution  $\Delta^{13}\text{C}_{\text{bulk}}$  record using  
83  $\delta^{13}\text{C}_{\text{TOC}}$  determined for 114 samples through a 90-m sequence (Fig. 3a).

84 The  $\delta^{13}\text{C}_{\text{carb}}$  and  $\delta^{13}\text{C}_{\text{TOC}}$  profiles display all eight carbon isotope segments  
85 previously identified to be global<sup>23</sup> that are placed in a tight framework of  
86 biostratigraphy<sup>18,19</sup> with the characteristic negative and subsequent positive excursions  
87 related to the input of depleted carbon to the ocean-atmosphere and subsequent  
88 enhanced carbon burial under global greenhouse conditions (Fig. 2). The absolute  
89 values as well as the overall shape of the  $\delta^{13}\text{C}_{\text{carb}}$  curve, including the magnitude of  
90 the positive and negative excursion, are similar to those recorded around the globe  
91 (Fig. S1 and S2).

92 Biomarkers such as short-chain *n*-alkanes ( $\text{C}_{17}$  and  $\text{C}_{18}$ ) and pristane and  
93 phytane, the latter two derived from phytyl side chains of the chlorophylls of algae  
94 and cyanobacteria, can serve as proxies for the isotopic composition of  
95 phytoplankton<sup>10,24</sup>. A lower-resolution record of compound-specific  $\delta^{13}\text{C}$  from Cau  
96 was generated using these biomarkers (Fig. 2b), which in our samples predominantly  
97 derive from algae ( $\delta^{13}\text{C}_{\text{alg}}$ ).  $\delta^{13}\text{C}_{\text{alg}}$  was determined for a total of 19 samples and range  
98 from -24 to -34.5 ‰ (or -20 to -30.5 ‰ when corrected to bulk biomass), with the  
99 lowest values during the later stage of isotope segments C3 and C4 (Fig. 2b). The  
100 shapes as well as absolute values of  $\delta^{13}\text{C}_{\text{alg}}$  are very similar to  $\delta^{13}\text{C}_{\text{TOC}}$ , indicating that

101  $\delta^{13}\text{C}_{\text{TOC}}$  is not significantly influenced by changes in the composition of bulk organic  
102 matter via either changes in source input or diagenesis. This suggests that the majority  
103 of organic matter at Cau is of marine (algal) origin, which is consistent with the  
104 overall biomarker assemblage<sup>20</sup>.

105 The  $\delta^{13}\text{C}_{\text{alg}}$  values are also similar to those reported from other (low-  
106 resolution) records across OAE 1a. Taken together this demonstrates that the  $\delta^{13}\text{C}_{\text{alg}}$   
107 we report from Cau are typical for OAE 1a. The similarity of  $\delta^{13}\text{C}_{\text{alg}}$  compared to  
108 other OAE 1a records together with the absence of major changes in total organic  
109 carbon content (Fig. S4) and biomarker distribution across OAE 1a suggest that  
110 changes in algal composition (Fig. S3), physiology, or nutrient contents of the waters  
111 are unlikely to have had a significantly effect, mitigating concerns associated with  
112 growth rate impacts on  $\delta^{13}\text{C}$  records. The negative shift in  $\delta^{13}\text{C}_{\text{TOC}}$  values, similar to  
113 that seen in  $\delta^{13}\text{C}_{\text{alg}}$ , and resulting positive excursion in the  $\Delta^{13}\text{C}_{\text{bulk}}$  record between 55  
114 and 90 m therefore predominantly indicates a greater discrimination against  $^{13}\text{C}$   
115 during algal photosynthesis due to elevated  $p\text{CO}_2$  levels (Fig. 3a).

116 Using  $\delta^{13}\text{C}_{\text{alg}}$  we then tentatively quantified  $p\text{CO}_2$  by converting  $\Delta^{13}\text{C}$  values  
117 into  $\epsilon_p$  (carbon isotope discrimination during photosynthesis) and using modern  
118 relationships between  $\epsilon_p$  and  $\{\text{CO}_2(\text{aq})\}$ . The absolute  $\text{CO}_2$  values are calculated using  
119 a number of assumptions for palaeoproductivity, sea surface temperature, and  
120 equilibrium  $\text{CO}_2$  exchange between ocean and atmosphere and should be considered  
121 as estimates. Pre-OAE 1a values are estimated between 800 and 1200 ppmv (Fig. 3b),  
122 entirely consistent with low-resolution multi-proxy estimates of (Early) Cretaceous  
123 background  $p\text{CO}_2$ <sup>13,25</sup>. During OAE 1a, specifically the latter part of segment C3-C4,  
124  $p\text{CO}_2$  doubled to values between 1400 and 2800 ppmv. We support the minimum  
125  $p\text{CO}_2$  values during segment C3 and maximum  $p\text{CO}_2$  values during segment C4 by

126 providing low-resolution independent  $p\text{CO}_2$  estimates from the Djebel Serdj section  
127 from Tunisia<sup>26</sup> (Fig. 3b). The values, which were obtained using compound-specific  
128  $\delta^{13}\text{C}_{\text{alg}}$  and the exact same assumptions as used to calculate  $p\text{CO}_2$  at Cau, range  
129 between 1100 and 2000 ppmv with the highest values during C4. The similarity in  
130 absolute  $p\text{CO}_2$  values between the two records demonstrates that the high-resolution  
131  $p\text{CO}_2$  record from Cau represents a global signal and is not significantly biased by  
132 local factors. It is important to note that due to the non-linear nature of the  $\epsilon_p$  and  
133  $\{\text{CO}_2(\text{aq})\}$ -relationship the higher  $p\text{CO}_2$  values could be underestimates.

134 The  $p\text{CO}_2$  record for the first time depicts the often-inferred increase and  
135 decrease in  $p\text{CO}_2$  across segments later part of C3 to mid-C7 (Fig. 3a-b). As segments  
136 C3-C6 (OAE 1a) are estimated to represent around 1.1 Myrs and segment C7 an  
137 additional 1.6 Myrs<sup>15</sup>, the period of elevated “super greenhouse”  $\text{CO}_2$  levels, likely  
138 lasted around 1.5 to 2 Myrs. The continuously high  $p\text{CO}_2$  values during segments C4-  
139 C6 suggest constant input of carbon into the ocean-atmosphere system, almost  
140 balanced by extensive organic matter burial in black shales around the world as  
141 indicated by the positive  $\delta^{13}\text{C}_{\text{carb}}$  excursion.

142 The timing of the  $p\text{CO}_2$  increase that starts in the middle of segment C3  
143 provides critical constraints on the source of excess  $\text{CO}_2$  during OAE 1a. Records  
144 from the Pacific and Tethys realms demonstrate that during OAE 1a the global  
145 oceanic Osmium (Os) isotope composition was exceptionally unradiogenic (mantle-  
146 like), interpreted to reflect the main phase of eruption of the Ontong Java plateau<sup>7,27</sup>.  
147 The major shift in Os-isotopes and hence eruption phase occurs well after the onset of  
148 the nannoconid crisis during the middle of segment C3, at the same time as the onset  
149 of  $\Delta^{13}\text{C}_{\text{bulk}}/p\text{CO}_2$  increase at Cau (Fig. 3c). The simultaneous shifts in Os-isotopes and

150  $p\text{CO}_2$  provides compelling evidence that the source of excess  $\text{CO}_2$  is derived from  
151 volcanic outgassing related to the emplacement of the Ontong Java Plateau.

152 In addition, the initial two-step rise in  $\Delta^{13}\text{C}_{\text{bulk}}/p\text{CO}_2$  during segment C3-C4  
153 spans roughly 10 meters in our section from 55 to 65 m (Fig. 3). Estimates from other  
154 expanded sections suggest a duration of 100-300 kyr for C3<sup>16,17</sup>, resulting in average  
155 sedimentation rates of 5 to 15 cm/kyr for this segment. Combined with the assumed  
156 duration of segment C4 of 200-280 kyr<sup>15</sup>, the  $\text{CO}_2$  doubling took at least 100 kyr and  
157 very likely more than 300 kyr.

158 Previous studies argued that the nanoconid crisis was caused by widespread  
159 and sustained surface ocean acidification due to numerous pulses of  $\text{CO}_2$  and  
160 methane, with the first pulse coinciding with the onset of the nanoconid crisis during  
161 carbon isotope segment C2<sup>5</sup>. However, our high-resolution  $p\text{CO}_2$  record challenges  
162 this. Our record indicates a gradual and sustained, two-step increase in  $p\text{CO}_2$ , likely  
163 volcanic sourced, during the latter part of segment C3 and C4 that took place over at  
164 least 100 kyr and occurred well after the onset of the nanoconid crisis. Such a slow  
165 ( $> 10$  kyr)  $\text{CO}_2$  release is buffered in the ocean by dissolution of carbonates in deep-  
166 sea sediments combined with silicate rock weathering on land and, assuming no major  
167 spatial shift in carbonate burial, would have prevented a coupled decline in pH and  
168  $\Omega^{28,29}$ . Due to current uncertainties in determining absolute ages or durations in the  
169 Early Cretaceous we cannot completely rule-out very brief episodes of surface ocean  
170 acidification during the latter part of segment C3 and C4 when  $p\text{CO}_2$  increases.  
171 However, the significant lag ( $\sim 10$  m, representing at least 60 kyr during C3) between  
172 the onset of the nanoconid crisis and onset of  $\text{CO}_2$  increase and shift in Os-isotopes  
173 (Fig. 3) clearly demonstrates that  $\text{CO}_2$ -induced surface ocean acidification could not  
174 have caused the nanoconid crisis.



175 In summary, our records demonstrate that OAE 1a was associated with a  
176 gradual, two-step increase in  $p\text{CO}_2$  to values roughly double that of pre-OAE 1a  
177 values. The similarity in timing between changes in  $p\text{CO}_2$  and oceanic Os-isotope  
178 inventory suggests that volcanic outgassing associated with the emplacement of the  
179 Ontong Java Plateau was the dominant source of  $\text{CO}_2$ . The prolonged duration of  
180  $p\text{CO}_2$  increase, and by extension the total amount of released carbon, indicates that  
181 methane release from gas hydrates was not likely a major source of  $p\text{CO}_2$  during OAE  
182 1a.

183

#### 184 References

- 185 1 Jenkyns, H. C. Geochemistry of oceanic anoxic events. *Geochem. Geophys.*  
186 *Geosy.* **11**, Q03004 (2010).
- 187 2 Mutterlose, J., Bottini, C., Schouten, S. & Sinninghe Damsté, J. S. High sea-  
188 surface temperatures during the early Aptian Oceanic Anoxic Event 1a in the  
189 Boreal Realm. *Geology* **42**, 439-442 (2014).
- 190 3 Ando, A., Kaiho, K., Kawahata, H. & Kakegawa, T. Timing and magnitude of  
191 early Aptian extreme warming: Unraveling primary  $\delta^{18}\text{O}$  variation in  
192 indurated pelagic carbonates at Deep Sea Drilling Project Site 463, central  
193 Pacific Ocean. *Palaeogeogr., Palaeoclimatol., Palaeoecol.* **260**, 463-476  
194 (2008).
- 195 4 Erba, E. Nannofossils and Superplumes: The Early Aptian "Nannoconid  
196 Crisis". *Paleoceanography* **9**, 483-501 (1994).
- 197 5 Erba, E., Bottini, C., Weissert, H. J. & Keller, C. E. Calcareous  
198 Nannoplankton Response to Surface-Water Acidification Around Oceanic  
199 Anoxic Event 1a. *Science* **329**, 428-432 (2010).
- 200 6 Méhay, S. *et al.* A volcanic  $\text{CO}_2$  pulse triggered the Cretaceous Oceanic  
201 Anoxic Event 1a and a biocalcification crisis. *Geology* **37**, 819-822 (2009).
- 202 7 Bottini, C., Cohen, A. S., Erba, E., Jenkyns, H. C. & Coe, A. L. Osmium-  
203 isotope evidence for volcanism, weathering, and ocean mixing during the early  
204 Aptian OAE 1a. *Geology* **40**, 583-586 (2012).
- 205 8 Kump, L. R., Bralower, T. J. & Ridgwell, A. Ocean acidification in deep time.  
206 *Oceanography* **22**, 94-107 (2009).
- 207 9 Gibbs, S. J., Robinson, S. A., Bown, P. R., Jones, T. D. & Henderiks, J.  
208 Comment on "Calcareous Nannoplankton Response to Surface-Water  
209 Acidification Around Oceanic Anoxic Event 1a". *Science* **332**, 175 (2011).
- 210 10 Heimhofer, U., Hochuli, P. A., Herrle, J. O., Andersen, N. & Weissert, H.  
211 Absence of major vegetation and palaeoatmospheric  $p\text{CO}_2$  changes associated  
212 with oceanic anoxic event 1a (Early Aptian, SE France). *Earth Plant. Sc. Lett.*  
213 **223**, 303-318 (2004).
- 214 11 van Breugel, Y. *et al.* Synchronous negative carbon isotope shifts in marine  
215 and terrestrial biomarkers at the onset of the early Aptian oceanic anoxic event

- 216 1a: Evidence for the release of <sup>13</sup>C-depleted carbon into the atmosphere.  
217 *Paleoceanography* **22**, PA1210 (2007).
- 218 12 Beerling, D. J., Lomas, M. R. & Gröcke, D. R. On the nature of methane gas-  
219 hydrate dissociation during the Toarcian and Aptian Oceanic anoxic events.  
220 *Am. J. Sci.* **302**, 28-49 (2002).
- 221 13 Hönisch, B. *et al.* The Geological Record of Ocean Acidification. *Science* **335**,  
222 1058-1063 (2012).
- 223 14 Li, Y.-X. *et al.* Toward an orbital chronology for the early Aptian Oceanic  
224 Anoxic Event (OAE1a, ~ 120 Ma). *Earth Planet. Sc. Lett.* **271**, 88-100 (2008).
- 225 15 Malinverno, A., Erba, E. & Herbert, T. D. Orbital tuning as an inverse  
226 problem: Chronology of the early Aptian oceanic anoxic event 1a (Selli Level)  
227 in the Cismon APTICORE. *Paleoceanography* **25**, PA2203 (2010).
- 228 16 Kuhnt, W., Holbourn, A. & Moullade, M. Transient global cooling at the onset  
229 of early Aptian oceanic anoxic event (OAE) 1a. *Geology* **39**, 323-326 (2011).
- 230 17 Lorenzen, J. *et al.* A new sediment core from the Bedoulian (Lower Aptian)  
231 stratotype at Roquefort-La Bédoule, SE France. *Cretaceous Res.* **39**, 6-16  
232 (2013).
- 233 18 de Gea, G. A., Castro, J. M., Aguado, R., Ruiz-Ortiz, P. A. & Company, M.  
234 Lower Aptian carbon isotope stratigraphy from a distal carbonate shelf setting:  
235 the Cau section, Prebetic zone, SE Spain. *Palaeogeogr., Palaeoclimatol.,*  
236 *Palaeoecol.* **200**, 207-219 (2003).
- 237 19 Aguado, R., Castro, J. M., Company, M. & Alfonso De Gea, G. Aptian bio-  
238 events—an integrated biostratigraphic analysis of the Almadich Formation,  
239 Inner Prebetic Domain, SE Spain. *Cretaceous Res.* **20**, 663-683 (1999).
- 240 20 Quijano, M. L. *et al.* Organic geochemistry, stable isotopes, and facies  
241 analysis of the Early Aptian OAE-New records from Spain (Western Tethys).  
242 *Palaeogeogr., Palaeoclimatol., Palaeoecol.* **365-366**, 276-293 (2012).
- 243 21 Kump, L. R. & Arthur, M. A. Interpreting carbon-isotope excursions:  
244 carbonates and organic matter. *Chem. Geol.* **161**, 181-198 (1999).
- 245 22 Jarvis, I., Lignum, J. S., Gröcke, D. R., Jenkyns, H. C. & Pearce, M. A. Black  
246 shale deposition, atmospheric CO<sub>2</sub> drawdown, and cooling during the  
247 Cenomanian-Turonian Oceanic Anoxic Event. *Paleoceanography* **26**, PA3201  
248 (2011).
- 249 23 Menegatti, A. P. *et al.* High-Resolution  $\delta^{13}\text{C}$  Stratigraphy Through the Early  
250 Aptian "Livello Selli" of the Alpine Tethys. *Paleoceanography* **13**, 530-545  
251 (1998).
- 252 24 Sinninghe Damsté, J. S., Kuypers, M. M. M., Pancost, R. D. & Schouten, S.  
253 The carbon isotopic response of algae, (cyano)bacteria, archaea and higher  
254 plants to the late Cenomanian perturbation of the global carbon cycle: Insights  
255 from biomarkers in black shales from the Cape Verde Basin (DSDP Site 367).  
256 *Org. Geochem.* **39**, 1703-1718 (2008).
- 257 25 Royer, D. L., Pagani, M. & Beerling, D. J. Geobiological constraints on Earth  
258 system sensitivity to CO<sub>2</sub> during the Cretaceous and Cenozoic. *Geobiology* **10**,  
259 298-310 (2012).
- 260 26 Heldt, M., Bachmann, M. & Lehmann, J. Microfacies, biostratigraphy, and  
261 geochemistry of the hemipelagic Barremian–Aptian in north-central Tunisia:  
262 Influence of the OAE 1a on the southern Tethys margin. *Palaeogeogr.,*  
263 *Palaeoclimatol., Palaeoecol.* **261**, 246-260 (2008).
- 264 27 Tejada, M. L. G. *et al.* Ontong Java Plateau eruption as a trigger for the early  
265 Aptian oceanic anoxic event. *Geology* **37**, 855-858 (2009).

- 266 28 Ridgwell, A. & Schmidt, D. N. Past constraints on the vulnerability of marine  
267 calcifiers to massive carbon dioxide release. *Nature Geosci.* **3**, 196-200  
268 (2010).  
269 29 Uchikawa, J. & Zeebe, R. E. Examining possible effects of seawater pH  
270 decline on foraminiferal stable isotopes during the Paleocene-Eocene Thermal  
271 Maximum. *Paleoceanography* **25**, PA2216 (2010).  
272

### 273 **Acknowledgements**

274 BDAN received funding through a Rubicon fellowship, awarded by the Netherlands  
275 Organisation for Scientific Research (NWO). Additional funding came from the  
276 advanced ERC grant “The greenhouse earth system” (T-GRES). JMC and MLQ were  
277 funded by University of Jaén fellowships, DNS was funded by a Royal Society URF.  
278 RDP and DNS acknowledge the Royal Society Wolfson Research Merit Award. We  
279 wish to thank the University of Jaén (CICT) for the use of analytical facilities and  
280 NERC for partial funding of the mass spectrometry facilities at the University of  
281 Bristol (contract no. R8/H10/63; [www.lsmsf.co.uk](http://www.lsmsf.co.uk)). Matthias Heldt is thanked for  
282 providing the samples from Djebel Serdj. This work is a contribution of the research  
283 project CGL2009-10329 and CGL2014-55274-P (Spanish Ministry of Science and  
284 Technology), “Episodios de Cambio Climático Global” (Instituto de Estudios  
285 Giennenses) and RNM-200 (Junta de Andalucía).  
286

### 287 **Author contributions**

288 BDAN, DNS, and RDP designed the study. JMC and GAD generated the stratigraphy,  
289 gathered the samples in the field, and prepared the samples for bulk stable isotope  
290 analyses. MLQ and JMC conducted the biomarker extraction and characterization of  
291 samples from Cau. BDAN performed the biomarker extraction of samples from  
292 Djebel Serdj, measured all compound specific isotope data for Cau and Djebel Serdj,  
293 and wrote the manuscript with contribution from all authors.  
294

### 295 **Competing financial interested**

296 We declare no competing financial interests.  
297

### 298 **Figure Legends**

#### 299 **Figure 1; Study area**

300 Palaeogeographic reconstruction of the Tethys region during the Aptian. The  
301 approximated locations of Cau and Djebel Serdj, as well as other key-OAE 1a

302 sections are indicated by red and black stars, respectively. Figure modified from R.  
303 Blakey, <http://cpgeosystems.com/euromaps.html>.

304

305 **Figure 2; Carbon isotope records from Cau across OAE 1a**

306 a) bulk carbonate stable carbon isotopes (light blue circles) and b) total organic matter  
307 stable carbon isotopes (dark blue circles) together with compound specific stable  
308 carbon isotopes of pristane (green circles), phytane (red diamonds), C<sub>17</sub> (orange  
309 triangles) and C<sub>18</sub> *n*-alkanes (brown reversed triangles). Error bars on compound  
310 specific stable carbon isotope data reflect 1σ of replicates. Isotope segments according  
311 to Menegatti et al.<sup>23</sup>. δ<sup>13</sup>C<sub>alg</sub> is corrected to bulk biomass by adding 4 ‰.

312

313 **Figure 3; Estimates of atmospheric CO<sub>2</sub> across OAE 1a**

314 a) High-resolution of Δ<sup>13</sup>C<sub>bulk</sub> at Cau together with b) *p*CO<sub>2</sub> estimate based on δ<sup>13</sup>C<sub>alg</sub>  
315 from Cau (orange diamonds) and Djebel Serdj (purple circles), and c) <sup>187</sup>Os/<sup>188</sup>Os  
316 record from Cismon<sup>7</sup>. The duration of the nannoconid crisis at Cau<sup>19</sup> and Cismon<sup>5</sup> is  
317 indicated by green bars. Turquoise shading in a) represent uncertainty in Δ<sup>13</sup>C<sub>bulk</sub>,  
318 orange shading in b) represents the uncertainty in *p*CO<sub>2</sub>-estimates related to  
319 uncertainty in δ<sup>13</sup>C<sub>carb</sub> and growth rate and cell geometry (the *b*-value), while light-  
320 yellow shading is the superimposed spread in the different δ<sup>13</sup>C<sub>alg</sub> for a specific  
321 sample.

322 **Material and methods**

323 **Data collection**

324 The Cau section was completed re-logged and remeasured. Bulk C-isotope analyses  
325 of the carbonate fraction ( $\delta^{13}\text{C}_{\text{carb}}$ ) were carried out at the Stable Isotope Laboratory of  
326 the University of Michigan, using a Finnigan MAT Kiel IV preparation device  
327 coupled directly to the inlet of a Finnigan MAT 253 triple collector isotope ratio mass  
328 spectrometer. The international carbonate standard NBS-19 was used to calibrate to  
329 V-PDB, with an average precision of 0.15 ‰. The C-isotope analyses of the total  
330 organic fraction ( $\delta^{13}\text{C}_{\text{TOC}}$ ) were performed at the Stable Isotope Laboratory (SIDI) of  
331 the Universidad Autónoma of Madrid. Samples were treated with 3% HCL for 24  
332 hours to remove carbonates and then analysed with an Carlo Erba 1108 elemental  
333 analyser coupled to a IRMS VG Isochrom in continuous flow mode. The results were  
334 calibrated to the VPDB standard, with a precision better than 0.1 ‰.

335 Samples for compound specific C-isotopes ( $\delta^{13}\text{C}_{\text{alg}}$ ) from Cau were extracted  
336 at the University of Jaén. Around 10 grams of grounded bulk sample was extracted  
337 using Dionex automated solvent extraction (ASE) and a mixture of dichloromethane  
338 (DCM) and methanol (MeOH) (8:2). The ASE program consisted of three 5 min  
339 cycles at 100 °C and 10 atm. The five samples from Djebel Serdj (Tunisia) were  
340 extracted at the University of Bristol using soxhlet apparatus. Between 30 and 40  
341 grams of grounded bulk sample was extracted with a mixture of dichloromethane  
342 (DCM) and methanol (MeOH) (2:1) for 24 hrs. The total lipid extracts of samples  
343 from both locations were concentrated and separated into three fractions using silica  
344 open column chromatography. Successive elution with 3 ml of hexane, 4 ml  
345 hexane/DCM (9:1 v/v) and 4 ml of MeOH resulted in saturated hydrocarbon, aromatic  
346 and polar fractions, respectively. Compound specific  $\delta^{13}\text{C}$  values of the saturated  
347 hydrocarbons were determined using an Isoprime 100 GC-combustion-isotope ratio  
348 MS (GC-C-IRMS) system at the University of Bristol. Samples were measured in  
349 duplicate and  $\delta^{13}\text{C}$  values were converted to Vienna Peedee Belemnite (VPDB) by  
350 bracketing with an in-house gas ( $\text{CO}_2$ ) of known  $\delta^{13}\text{C}$  value. Instrument stability was  
351 monitored by regular analysis of an in-house fatty acid methyl ester standard mixture;  
352 long-term precision is  $\pm 0.3$  ‰. Injection volume was 2  $\mu\text{l}$  on to a Zebtron-I non-polar  
353 column (50 m x 0.32 mm i.d., 0.10  $\mu\text{m}$  film thickness). The GC oven program was: 70  
354 °C (1 min hold), to 130 °C at 20 °C/min, then to 300 °C at 4 °C/min, and a final hold  
355 for 25 minutes at 300 °C. Samples were automatically integrated using the  
356 IonVantage software package.

357

358  **$p\text{CO}_2$  calculations using compound specific  $\delta^{13}\text{C}_{\text{alg}}$**

359 Popp et al.<sup>30,31</sup> demonstrated that for several species of marine phytoplankton, and  
360 assuming that  $\text{CO}_2(\text{aq})$  enters the cell via diffusion only, which is likely during the  
361 high  $\text{CO}_2$  world of the Cretaceous<sup>32</sup>, the isotopic effect associated with the  
362 photosynthetic fixation of carbon ( $\epsilon_p$ ) depends on the concentration of  $\text{CO}_2(\text{aq})$ ,  
363 growth rate, and cell geometry.

364

$$(1) \epsilon_p = \epsilon_f - \frac{b}{[\text{CO}_2(\text{aq})]}$$

365

366 With  $b$  being the combined species-specific factors that reflect physiological factors,  
367 including growth rate and cell geometry, and  $\epsilon_f$  being the maximum isotopic  
368 fractionation associated with the photosynthetic fixation of carbon, which is 25 ‰ for  
369 algae<sup>33</sup>.

370 Assuming surface waters were in equilibrium with the atmosphere,  
 371 atmospheric  $pCO_2$  can be calculated using Henry's law:  
 372

$$(2) pCO_2(ppmv) = \frac{[CO_2(aq)]}{K_o}$$

373

374 With  $K_o$ , the solubility constant, depending on temperature and salinity.  
 375

$$(3) \ln K_o \text{ (moles/l/atm)} \\ = A_1 + A_2 \frac{100}{T} + A_3 \ln \frac{T}{100} + S \left[ B_1 + B_2 \frac{T}{100} + B_3 \left( \frac{T}{100} \right)^2 \right]$$

376

377 With T = temperature (Kelvin), S = salinity (‰),  $A_1 = -58.0931$ ,  $A_2 = 90.5069$ ,  $A_3 =$   
 378  $22.2940$ ,  $B_1 = 0.027766$ ,  $B_2 = -0.025888$ ,  $B_3 = 0.0050578$ <sup>34</sup>  
 379

380

381 Based on this model, a large number of studies have used bulk organic matter  
 382 ( $\delta^{13}C_{TOC}$ ) and compound specific  $\delta^{13}C$  values to calculate  $\epsilon_p$  and/or  $pCO_2$  throughout  
 383 geological time<sup>35-39</sup>, including the Cretaceous and the OAEs<sup>6,10,22,24,40,41</sup>.

384

385 Here we calculated  $pCO_2$  using  $\delta^{13}C_{alg}$  based on four different marine  
 386 biomarker lipids ( $C_{17}$  and  $C_{18}$  *n*-alkanes and pristane and phytane) to generate a high  
 387 resolution record from Cau and a low-resolution at Djebel Serdj. Biomarkers such as  
 388 pristane and phytane, derived from phytol side chains of the chlorophylls of algae and  
 389 cyanobacteria, are robust proxies for the isotopic composition of phytoplankton<sup>10,42</sup>.

390

391  $\epsilon_p$  depends on the isotopic difference between dissolved (aq)  $CO_2$  ( $\delta_d$ ) and  
 392 primary photosynthate ( $\delta_p$ )<sup>40</sup>.

393

$$(4) \epsilon_p = 10^3 \left[ \frac{\delta_d + 1000}{\delta_p + 1000} - 1 \right]$$

394

395 We calculated the isotopic composition of primary photosynthate ( $\delta_p$ ) using the  
 396 compound-specific isotopic composition ( $\delta^{13}C_{alg}$ ) and taking into the isotopic offset  
 397 between biomarker lipids and biomass ( $\Delta\delta$ ), which is assumed to be 4 ‰ for pristane  
 398 and phytane<sup>24,41-43</sup>. In our samples  $\delta^{13}C$  values of the short-chain *n*-alkanes are very  
 399 similar to those of pristane and phytane (average offset 0.4 ‰), in-line with findings  
 400 from other OAEs<sup>44</sup>, and we therefore assumed  $\Delta\delta$  to be 4 ‰ for all four compounds.  
 401

402

$$(5) \delta_p = \delta^{13}C_{TOC} = \delta^{13}C_{alg} + \Delta\delta = \delta^{13}C_{alg} + 4 \text{ ‰}$$

403

404 The isotopic composition of dissolved  $CO_2$  ( $\delta_d$ ) was calculated using the isotopic  
 405 composition of bulk carbonate ( $\delta^{13}C_{carb}$ ), the calcite-bicarbonate enrichment of 1 ‰<sup>45</sup>  
 406 and the temperature dependent carbon isotopic fractionation of dissolved  $CO_2$  with  
 407 respect to  $HCO_3^-$  ( $\epsilon_{b(a)}$ )<sup>46</sup>.

408

$$(6) \delta_d = \delta^{13}C_{carb} - 1 + \epsilon_{b(a)}$$

409

$$(7) \epsilon_{b(a)} = 24.12 - \frac{9866}{T}$$

410

411 **Uncertainties in  $pCO_2$  estimates**

408 The absolute CO<sub>2</sub> values are calculated using a number of assumptions for  
409 palaeoproductivity, sea surface temperature, and equilibrium CO<sub>2</sub> exchange between  
410 ocean and atmosphere and should be considered as estimates. Below we discuss these  
411 assumptions and their impact on the absolute pCO<sub>2</sub> estimates. Importantly our main  
412 conclusions depend on the timing of changes in pCO<sub>2</sub> and are valid independent of the  
413 absolute CO<sub>2</sub> estimates or magnitude of change.

414

#### 415 *Fidelity of the bulk $\delta^{13}\text{C}_{\text{carb}}$*

416 The first assumption is that bulk  $\delta^{13}\text{C}_{\text{carb}}$  at Cau reflects the isotopic composition of  
417 dissolved (aq) CO<sub>2</sub> ( $\delta_{\text{d}}$ ), which directly impacts  $\epsilon_{\text{p}}$  (see eq. 4 and 6). First, the  $\delta^{13}\text{C}$   
418 composition of carbonate rocks is much more resistant to chemical overprinting than  
419  $\delta^{18}\text{O}$ , such that even clearly diagenetically altered and dolomitized carbonates appear  
420 to preserve their original  $\delta^{13}\text{C}$  composition<sup>47</sup>, including OAE 1a sections<sup>48</sup>. In addition,  
421 nanofossil-dominated bulk carbonate  $\delta^{13}\text{C}$  is a reliable recorder of  $\delta^{13}\text{C}_{\text{DIC}}$  in pre-  
422 Cenozoic sediments<sup>49</sup> and  $\delta^{13}\text{C}_{\text{carb}}$  is well-suited for global correlation during OAEs<sup>3</sup>.  
423 As a result the shape of the  $\delta^{13}\text{C}_{\text{carb}}$  curves and magnitude of the positive and negative  
424 carbon isotope excursion across OAE 1a is similar across the globe (and in a range of  
425 depositional settings). In fact because black shale deposition is asynchronous, most  
426 authors use  $\delta^{13}\text{C}$  chemostratigraphy and the C-isotope segments defined by Menegatti  
427 et al.<sup>23</sup> to correlate OAE 1a records across the globe<sup>1,14,15,48,50</sup>. Published  $\delta^{13}\text{C}_{\text{carb}}$   
428 records may appear different in shape and magnitude but this apparent difference  
429 between sections is to a large extent due to visual comparison of expanded to  
430 condensed sections.

431 To demonstrate that our  $\delta^{13}\text{C}_{\text{carb}}$  record from Cau is similar in shape and  
432 magnitude of excursions to other records, we compare the record from Cau to the  
433  $\delta^{13}\text{C}_{\text{carb}}$  of a similarly expanded section from southeast France<sup>16</sup> (Fig. S1). The reason  
434 for choosing this record is that it is one of the few other expanded OAE 1a sections.  
435 We subsequently tuned the  $\delta^{13}\text{C}_{\text{carb}}$  from SE France record to the one from Cau other  
436 using four tie-points. Three are based on biostratigraphy and one on the boundary of  
437 the C4/C5-isotope segment. Figure S2 clearly demonstrates the similarity in shape and  
438 magnitude of excursion of the two  $\delta^{13}\text{C}_{\text{carb}}$  curves. The similarity between the two  
439  $\delta^{13}\text{C}_{\text{carb}}$  curves, located around 1000 km apart, suggests that the  $\delta^{13}\text{C}_{\text{carb}}$  record from  
440 Cau is not significantly influenced by diagenesis or other secondary effects but  
441 reflects a  $\delta^{13}\text{C}_{\text{DIC}}$  signal and can be used to calculate  $\delta_{\text{d}}$ . Even so, we assume a 0.5 ‰  
442 uncertainty in this in our uncertainty estimates (see further below).

443

#### 444 *Changes in algal composition and physiology*

445 Changes in the algal composition or physiology can affect  $\delta^{13}\text{C}_{\text{alg}}$  and  $\delta^{13}\text{C}_{\text{TOC}}$  and  
446 hence ultimately our pCO<sub>2</sub> estimates. To assess whether these factors changed across  
447 OAE 1a at Cau, we determined the relative C<sub>27</sub>-C<sub>30</sub>  $\alpha\alpha\alpha\text{R}$  sterane distribution in all  
448 samples. Steranes are derived from algal-derived steroids and sterols, such that their  
449 relative distribution in the geological record is often used to infer changes in algal  
450 composition<sup>51,52</sup>. In addition, the sterol, and hence sterane, composition can be  
451 influenced by environmental factors such as light intensity, temperature, and growth  
452 stage<sup>53</sup>.

453 Our results show that the sterane distribution varied little across OAE 1a and  
454 changes do not coincide with major changes in  $\delta^{13}\text{C}$  (Fig. S3). This provides strong  
455 evidence against significant changes in algal composition and/or environmental  
456 factors at Cau during OAE 1a influencing  $\delta^{13}\text{C}$ . This is in-line with the lack of a  
457 temperature change in the low-latitudes during OAE 1a as indicated by our TEX<sub>86</sub>

458 estimates from Site 398, as well as the minimal change in TOC content (Fig. S4).  
459 Taken together, changes in algal composition and/or variations in physiology due to  
460 changing environmental factors are unlikely to have had a significantly effect.  
461 Although more tentative, the lack of any change in algal assemblage suggests that  
462 there were no dramatic changes in the nutrient contents of the waters, mitigating  
463 concerns associated with growth rate impacts on  $\delta^{13}\text{C}$  records.

464

#### 465 *Comparison to published records of $\delta^{13}\text{C}_{\text{alg}}$ and $\epsilon_p$*

466 The  $\delta^{13}\text{C}_{\text{alg}}$  from Cau (as well as Djebel Serdj, Fig. S8) are similar to those reported  
467 from other (low-resolution) sections across OAE 1a. Van Breugel et al.<sup>11</sup> provide  $\delta^{13}\text{C}$   
468 of pristane across part of OAE 1a at Cismon. Their values range between -28 and -35  
469 ‰, similar to the values we measured at Cau (-29 to -34.5 ‰ for pristane) and low-  
470 resolution record of Djebel Serdj (-29.2 to -32.6 ‰ for pristane). For the last  $\pm 50$   
471 Myr, numerous biomarker-based  $p\text{CO}_2$  records are based on  $\delta^{13}\text{C}$  of alkenones<sup>35,37</sup>.  
472 Although alkenones are generally not found in Cretaceous sediments, the first  
473 occurrence of alkenones actually is in the extremely organic rich OAE 1a section at  
474 Shatsky Rise (ODP Site 1213)<sup>54</sup>. The isotopic composition of these alkenones was  
475 determined in one sample ( $\sim -32$  ‰)<sup>55</sup>, similar to the minimum values we determined,  
476 and again demonstrate that the  $\delta^{13}\text{C}_{\text{alg}}$  we report are typical for OAE 1a.

477 None of these studies calculated  $\epsilon_p$ . At Shatsky, no  $\delta^{13}\text{C}_{\text{carb}}$  is available.  
478 Cismon is characterized by large variations in the source of organic matter<sup>11</sup> and  
479  $\text{TEX}_{86}$  is influenced by thermal maturity<sup>56</sup>. Heimhofer et al.<sup>10</sup> used, among others,  $\text{C}_{17}$   
480 and  $\text{C}_{18}$  short-chain  $n$ -alkanes to reconstruct  $\epsilon_p$  across segment C5 to C7 in the Serre  
481 Chaitieu section from France (Fig. S6). For this part of OAE 1a the  $\delta^{13}\text{C}$  of the short-  
482 chain  $n$ -alkanes in the Serre Chaitieu section ranges between -32 and -27 ‰, similar  
483 to our estimates for these compounds across segments C5-C7 at Cau (-32 to -25 ‰)  
484 and low-resolution record of Djebel Serdj (-27.9 to -31.8 ‰). Their estimates of  $\epsilon_p$ ,  
485 although not depicting the increase in  $p\text{CO}_2$  as there are no data from segments C3  
486 and C4, with maximum  $\epsilon_p$  values of around 22‰ are very similar to our maximum  $\epsilon_p$   
487 values across this period (maximum  $\epsilon_p$  at Cau and Djebel Serdje are  $\sim 22$ ‰ during  
488 C4-C6), markedly higher than any values yet to be reported for the last 15 million  
489 years<sup>35</sup>. We therefore conclude that our  $\delta^{13}\text{C}_{\text{alg}}$  and  $\epsilon_p$  estimates are typical for OAE  
490 1a, and reflect a global signal.

491

#### 492 *Estimating the $b$ -value*

493 The growth rate and cell geometry impact the isotopic effect expressed during the  
494 photosynthetic fixation of carbon ( $\epsilon_p$ )<sup>31,33</sup>. These effects are combined into the  
495 constant  $b$  and have an impact on the absolute  $p\text{CO}_2$  estimates. In the modern ocean,  $b$   
496 for haptophyte algae ranges from  $< 100$  in oligotrophic regions to  $> 200$  in upwelling  
497 regions<sup>33,57-59</sup>

498 Although it is not straightforward to estimate  $b$  during OAE 1a, previous  
499 estimates for the Late Cretaceous and OAE 2 assumed a value of 171<sup>24,41,43</sup>. This  
500 value is based on the proposed linear correlation between  $b$  and sedimentary bulk  $\delta^{15}\text{N}$   
501 values<sup>57</sup> and an assumed  $\delta^{15}\text{N}$  of -2 ‰ during the Late Cretaceous at Demerara rise<sup>41</sup>.

502

$$(8) \ b = 53.27 \left[ \frac{\delta^{15}\text{N} - 12.386}{-8.146} \right] + 77.21$$

503

504 Bulk  $\delta^{15}\text{N}$  values across OAE 1a yield similar negative values between -1 and -3  
505 ‰<sup>50,60</sup>, also suggesting a  $b$  value of  $\sim 171$ . This relationship is implicitly based on



506 modern ocean alkenone  $\delta^{13}\text{C}$  values and therefore is tuned for coccolithophorids;  
507 algae with different surface area to volume ratios or even different membrane  
508 diffusivity could have different  $b$  values<sup>61</sup>. This represents a first order limitation on  
509 the calculation of absolute  $p\text{CO}_2$  values. Nonetheless, Popp et al.<sup>31</sup> have shown that  
510 other photoautotrophs do exhibit similar relationships; as such, we can assume a  
511 constant  $b$  value of 171 for our  $p\text{CO}_2$  estimates but use a range of  $b$  values to  
512 constrain the uncertainty of the absolute values. Given the lack of evidence for  
513 changes in the algal community structure, we suggest that this has had minimal  
514 impact on our temporal trends.

515 Cau was not an upwelling site and is characterized by background TOC values  
516 between 0.5 and 1.5 %. Even during OAE 1a the period of increased organic matter  
517 burial was short lived and not very intense as indicated by the moderate and brief  
518 increase in TOC to maximum values of 2.5 % (Fig. S4), making it unlikely that the  $b$   
519 value was much higher. If  $b$  did increase, then this would have occurred during  
520 segments C3-C6 and accounting for it would yield higher  $p\text{CO}_2$  estimates at this time.

521

#### 522 *Estimating subtropical Sea Surface Temperatures (SSTs)*

523 Sea surface temperatures (SSTs) impact the estimated  $p\text{CO}_2$  in several ways, but  
524 predominantly from their influence on Henry's Law. Here we estimated SSTs using  
525 the  $\text{TEX}_{86}$  palaeothermometer, which is based on the distribution of isoprenoidal  
526 glycerol dialkyl glycerol tetraethers (GDGTs) in marine sediments<sup>62,63</sup>. The advantage  
527 of  $\text{TEX}_{86}$  over inorganic geochemical proxies is that  $\text{TEX}_{86}$  is less influenced by  
528 diagenesis, which for example can alter the primary  $\delta^{18}\text{O}$  signature of carbonates, and  
529 is not directly controlled by seawater chemistry such as  $\text{Mg}/\text{Ca}$  and  $\delta^{18}\text{O}$ , which very  
530 likely was different during the Cretaceous and especially OAEs.

531 We did not detect measurable amounts of GDGTs in the samples from Cau.  
532 Although the organic matter at Cau is thermally immature<sup>20</sup> with respect to oil  
533 generation, this is not necessarily the case with respect to the occurrence of GDGTs.  
534 Due to the presence of heteroatoms (i.e. the ether bond), GDGTs begin to degrade at  
535 relatively low thermal maturity<sup>64,65</sup>; in fact, they are uncommon in the maturation  
536 window when steranes, pristane and phytane have begun to be liberated from kerogen.

537 To overcome this issue, we obtained  $\text{TEX}_{86}$ -based SST estimates from DSDP  
538 Site 398 across OAE 1a. Site 398 is located in the North Atlantic, slightly north of  
539 Cau (Fig. 1), and covers OAE 1a<sup>14</sup>. Importantly it contains abundant GDGTs. Using  
540 the  $\text{TEX}_{86}^{\text{H}}$ -calibration<sup>66</sup>, SSTs at Site 398 across OAE 1a (C3-C6) are remarkably  
541 warm and stable with values around 34.5 °C (Fig. S5c). Such high subtropical SSTs  
542 are consistent with a large range of proxy-evidence that indicates that the Cretaceous  
543 was characterized by a hot greenhouse climate<sup>67-70</sup>. In addition, it closely ties-in with  
544 recent  $\text{TEX}_{86}^{\text{H}}$  estimates across OAE 1a from the mid-latitudes (~39 °N  
545 palaeolatitude) that range between 30 and 33 °C<sup>2</sup>, tropical SSTs in the Pacific that  
546 range between 31 and 38 °C during OAE 1a<sup>63,71</sup>, and high-latitude Southern Ocean (~  
547 55 °N palaeolatitude) SSTs of around 28 °C during OAE 1a<sup>69</sup>, which all indicate very  
548 high SSTs during OAE 1a with SSTs > 30 °C extending far into the mid-latitudes.

549 BIT-values, a proxy for the input of soil derived GDGTs<sup>72</sup>, vary between 0.06  
550 and 0.41 and there is no correlation between BIT-values and SSTs, arguing against a  
551 significant influence of terrestrial GDGTs on the  $\text{TEX}_{86}^{\text{H}}$  estimates. The organic  
552 matter at Site 398 across OAE 1a is thermally immature as indicated by the  $\text{C}_{31}$   
553 hopane  $\beta\beta/(\beta\beta+\beta\alpha+\alpha\beta)$  ratios that are always greater than 0.5 (Fig. S5d).

554 The reconstructed SSTs from Site 398 indicate a stable and warm subtropical  
555 climate, which appears inherent to greenhouse climates<sup>73</sup>. Based on the record from

556 Site 398, we assumed that subtropical SSTs across OAE 1a were relatively stable at  
557 Cau at 34.5 °C. Higher (36°C) or lower (30°C) SST estimates would lead to slightly  
558 different (max 250 ppmv) CO<sub>2</sub> values (Fig. S6). Assuming an increase in SSTs across  
559 OAE 1a, as seen in the higher latitudes<sup>2</sup>, would result in a slightly more pronounced  
560 increase in pCO<sub>2</sub> across OAE 1a.

561

### 562 *Uncertainty envelopes*

563 As explained above, our best pCO<sub>2</sub> estimates assume a *b*-value of 171, that δ<sup>13</sup>C<sub>carb</sub>  
564 reflects seawater δ<sup>13</sup>C<sub>DIC</sub>, and that SSTs in the subtropics were 34.5 °C. Assuming  
565 these parameters, pCO<sub>2</sub> was calculated for, where possible, all four biomarkers and an  
566 average of these estimates was plotted in figure 3 as a black line with orange data  
567 points.

568 To accurately incorporate the main sources of uncertainty in our pCO<sub>2</sub>  
569 calculations, largely associated with δ<sup>13</sup>C<sub>DIC</sub> determinations from δ<sup>13</sup>C<sub>carb</sub> that has an  
570 impact on ε<sub>p</sub> and uncertainty in the *b*-value due to growth rate and cell physiology that  
571 influences the absolute pCO<sub>2</sub> estimates, we calculated a minimum and maximum  
572 pCO<sub>2</sub> scenario. The minimum scenario assumes that δ<sup>13</sup>C<sub>carb</sub> overestimates seawater  
573 δ<sup>13</sup>C<sub>DIC</sub> by 0.5 ‰ and a low-end *b*-value of 150. The maximum scenario assumes that  
574 δ<sup>13</sup>C<sub>carb</sub> underestimates seawater δ<sup>13</sup>C<sub>DIC</sub> by 0.5 ‰ and a high-end *b*-value of 200.  
575 Note that uncertainty in δ<sup>13</sup>C<sub>carb</sub> manifest in ε<sub>p</sub>, which at Cau is similar compared to  
576 previous estimates<sup>10</sup> and other sites. A range from 150 to 200 for *b* was chosen as  
577 both Cau and Djebel Serdje are not upwelling sites and not characterized by large  
578 variations in TOC content or changes in algal composition and physiology. Assuming  
579 these parameters, pCO<sub>2</sub> was calculated for all four biomarkers. In figures 3 and S8,  
580 the orange shading represents the spread between the minimum and maximum pCO<sub>2</sub>  
581 estimates and, again, is the average value of all biomarker measurements (see Fig.  
582 S7). The light yellow shading represents the analytical uncertainty related to the  
583 compound specific δ<sup>13</sup>C measurements (e.g., how well does the average value of the  
584 four biomarkers represent the spread in compound specific δ<sup>13</sup>C) and represents 1σ  
585 from the average min. and max. pCO<sub>2</sub>-scenario (e.g. 1σ from the orange shading).

586 The uncertainty in Δ<sup>13</sup>C (the turquoise shading in figure 3), was calculated  
587 assuming both δ<sup>13</sup>C<sub>carb</sub> and δ<sup>13</sup>C<sub>TOC</sub> were as much as 0.5 ‰ too high or too low  
588 compared to seawater δ<sup>13</sup>C<sub>DIC</sub> and primary photosynthate δ<sup>13</sup>C, respectively, resulting  
589 in a combined error of 0.71 ‰ (√(0.5<sup>2</sup>+0.5<sup>2</sup>)).

590

### 591 **Duration of isotope segment C3**

592 Following Menegatti et al.<sup>23</sup> we defined C3 to span the decrease in bulk δ<sup>13</sup>C<sub>carb</sub>,  
593 covering the interval between 46 and 62 meter in our section (Fig. 2a). Identical to  
594 other OAE 1a records<sup>5,15,16</sup> the onset of the nannoconid crisis precedes the beginning  
595 of C3 at Cau. The first occurrence of *Schackoina cabri* at the top of C3 corresponds to  
596 what has been observed in other expanded sections<sup>16,17</sup>.

597 Previous estimates for the duration of C3 range from 20 to 45 kyr at  
598 Cismon<sup>14,15</sup>. However results from other more expanded sections demonstrate that  
599 this interval in Cismon is (highly) condensed and the duration of C3 was likely  
600 longer, with ranges between 100 and 300 kyr<sup>16,17,74,75</sup>. Recently the C3 interval at  
601 Cismon was also redefined, with an updated duration of between 100 and 200 kyr<sup>56</sup>.

602

### 603 **Duration of the reconstructed CO<sub>2</sub> input at Cau**

604 Even assuming a minimal duration of 20-45 ka for C3 as suggested by the original  
605 Cismon estimates<sup>14,15</sup>, the reconstructed CO<sub>2</sub> increase at Cau occurs across the later

606 part of C3 as well as the majority of C4, which lasted  $239 \pm 39$  kyr at Cismon<sup>15</sup>. This  
607 implies that independent of the exact duration of C3, the CO<sub>2</sub> increase occurred over  
608 at least 100 ka. Assuming a more likely duration of C3 of 100 to 300 kyr together  
609 with the duration of C4 of 239 ka, implies that the CO<sub>2</sub> increase at Cau likely  
610 occurred over more than 300 ka.

611

### 612 **Correlations to Cau**

613 We used the carbon isotope segment chemostratigraphy, originally developed by  
614 Menegatti et al.<sup>23</sup>, to compare the *p*CO<sub>2</sub> record from Djebel Serdj and Os-isotope  
615 record from Cismon to the records from Cau. For Cismon we used the updated  
616 definition of isotope segment C3 as used in Bottini et al.<sup>56</sup>. For the timing of the  
617 nanoconid crisis at Cismon we used the definition given in Malinverno et al.<sup>15</sup>. For  
618 Djebel Serdj we redefined the carbon isotope segments as shown in Figure S8, largely  
619 following Heldt et al.<sup>26</sup>. The low-resolution *p*CO<sub>2</sub> estimates from Djebel Serdj were  
620 plotted on top of those of Cau using a direct correlation. So for example, the estimates  
621 from the middle of segment C3 at Djebel Serdj are shown in the middle of C3 at Cau.  
622 The vertical error bars on the *p*CO<sub>2</sub> estimates from Djebel Serdj as shown in figure 3  
623 represents the uncertainty in this correlation.

624

### 625 **References:**

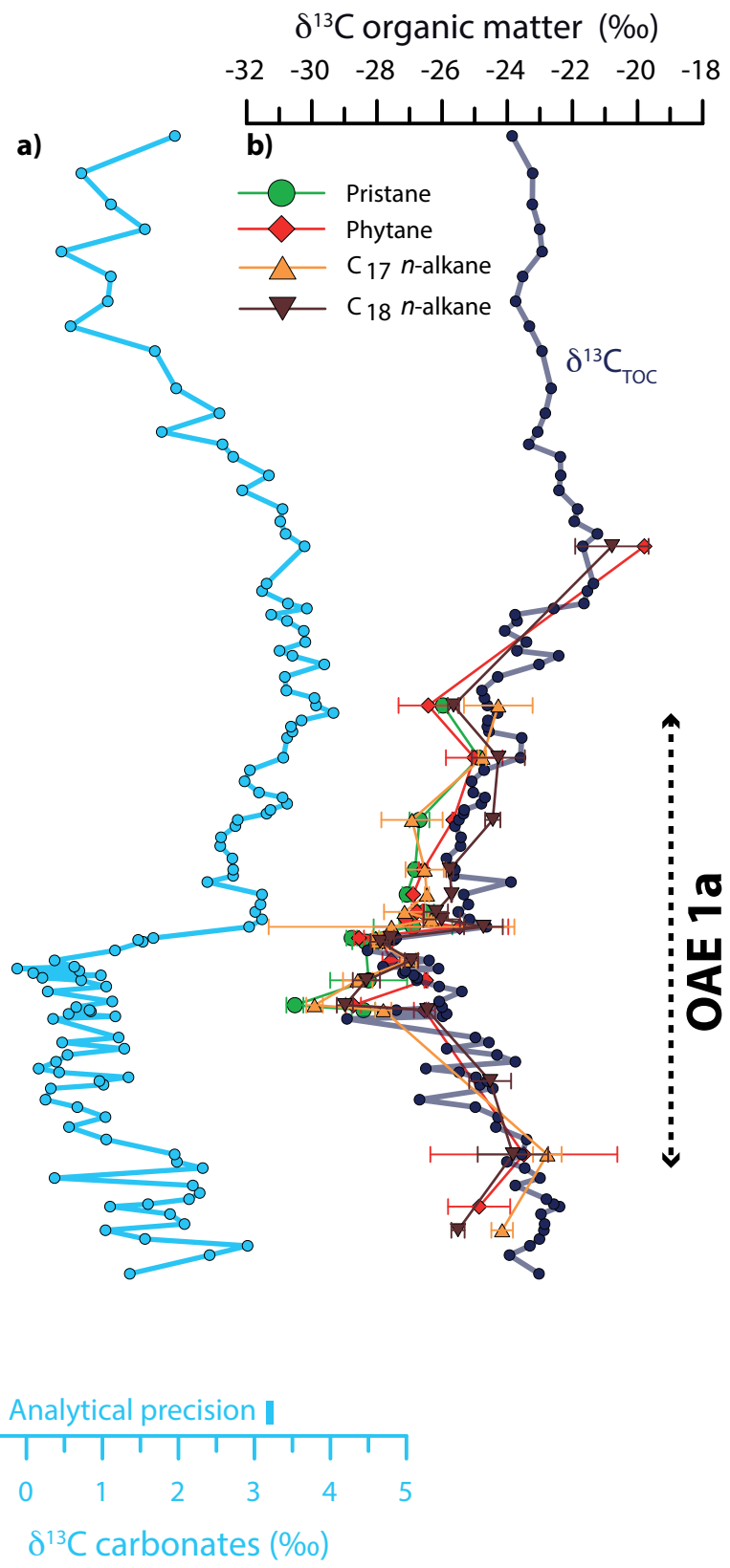
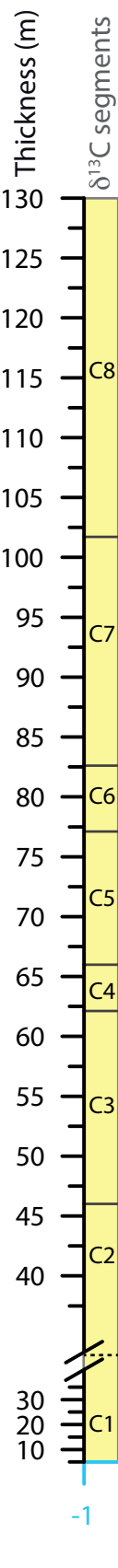
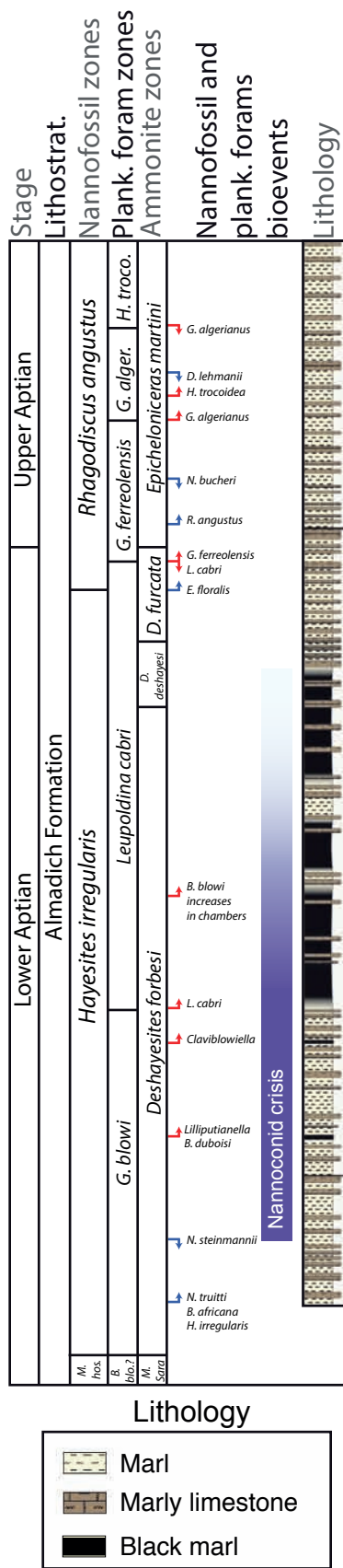
- 626 30 Popp, B. N., Takigiku, R., Hayes, J. M., Louda, J. W. & Baker, E. W. The  
627 post-Paleozoic chronology and mechanism of <sup>13</sup>C depletion in primary marine  
628 organic matter. *Am. J. Sc.* **289**, 436-454 (1989).
- 629 31 Popp, B. N. *et al.* Effect of Phytoplankton Cell Geometry on Carbon Isotopic  
630 Fractionation. *Geochim. Cosmochim. Ac.* **62**, 69-77 (1998).
- 631 32 Laws, E. A., Popp, B. N., Cassar, N. & Tanimoto, J. <sup>13</sup>C discrimination  
632 patterns in oceanic phytoplankton: likely influence of CO<sub>2</sub> concentrating  
633 mechanisms, and implications for palaeoreconstructions. *Funct. Plant Biol.* **29**,  
634 323-333 (2002).
- 635 33 Bidigare, R. R. *et al.* Consistent fractionation of <sup>13</sup>C in nature and in the  
636 laboratory: Growth-rate effects in some haptophyte algae. *Global Biogeochem.*  
637 *Cy.* **11**, 279-292 (1997).
- 638 34 Weiss, R. F. Carbon dioxide in water and seawater: the solubility of a non-  
639 ideal gas. *Mar. Chem.* **2**, 203-215 (1974).
- 640 35 Pagani, M., Zachos, J. C., Freeman, K. H., Tipple, B. & Bohaty, S. Marked  
641 Decline in Atmospheric Carbon Dioxide Concentrations During the Paleogene.  
642 *Science* **309**, 600-603 (2005).
- 643 36 Schoon, P. L., Sluijs, A., Sinninghe Damsté, J. S. & Schouten, S. Stable  
644 carbon isotope patterns of marine biomarker lipids in the Arctic Ocean during  
645 Eocene Thermal Maximum 2. *Paleoceanography* **26**, PA3215 (2011).
- 646 37 Seki, O. *et al.* Alkenone and boron-based Pliocene *p*CO<sub>2</sub> records. *Earth Plant.*  
647 *Sc. Lett.* **292**, 201-211 (2010).
- 648 38 Badger, M. P. S. *et al.* CO<sub>2</sub> drawdown following the middle Miocene  
649 expansion of the Antarctic Ice Sheet. *Paleoceanography* **28**, 42-53 (2013).
- 650 39 Raymo, M. E., Grant, B., Horowitz, M. & Rau, G. H. Mid-Pliocene warmth:  
651 stronger greenhouse and stronger conveyor. *Mar. Micropaleontol.* **27**, 313-326  
652 (1996).
- 653 40 Freeman, K. H. & Hayes, J. M. Fractionation of carbon isotopes by  
654 phytoplankton and estimates of ancient CO<sub>2</sub> levels. *Global Biogeochem. Cy.* **6**,  
655 185-198 (1992).

- 656 41 Bice, K. L. *et al.* A multiple proxy and model study of Cretaceous upper ocean  
657 temperatures and atmospheric CO<sub>2</sub> concentrations. *Paleoceanography* **21**,  
658 PA2002 (2006).
- 659 42 Schouten, S. *et al.* Biosynthetic effects on the stable carbon isotopic  
660 compositions of algal lipids: implications for deciphering the carbon isotopic  
661 biomarker record. *Geochim. Cosmochim. Ac.* **62**, 1397-1406 (1998).
- 662 43 van Bentum, E. C., Reichart, G. J., Forster, A. & Sinninghe Damsté, J. S.  
663 Latitudinal differences in the amplitude of the OAE-2 carbon isotopic  
664 excursion: pCO<sub>2</sub> and paleo productivity. *Biogeosciences* **9**, 717-731 (2012).
- 665 44 Schouten, S., van Kaam-Peters, H. M. E., Rijpstra, W. I. C., Schoell, M. &  
666 Sinninghe Damsté, J. S. Effects of an oceanic anoxic event on the stable  
667 carbon isotopic composition of early Toarcian carbon. *Am. J. Sci.* **300**, 1-22  
668 (2000).
- 669 45 Romanek, C. S., Grossman, E. L. & Morse, J. W. Carbon isotopic  
670 fractionation in synthetic aragonite and calcite: Effects of temperature and  
671 precipitation rate. *Geochim. Cosmochim. Ac.* **56**, 419-430 (1992).
- 672 46 Mook, W. G., Bommerson, J. C. & Staverman, W. H. Carbon isotope  
673 fractionation between dissolved bicarbonate and gaseous carbon dioxide.  
674 *Earth Plant. Sc. Lett.* **22**, 169-176 (1974).
- 675 47 Halverson, G. P., Hoffman, P. F., Schrag, D. P., Maloof, A. C. & Rice, A. H.  
676 N. Toward a Neoproterozoic composite carbon-isotope record. *Geol. Soc. Am.*  
677 *Bull.* **117**, 1181-1207 (2005).
- 678 48 Jenkyns, H. C. in *Proceedings of the Ocean Drilling Program, Scientific*  
679 *Results, vol. 143* (eds E.L. Winterer, W.W. Sager, J.V. Firth, & J.M. Sinton)  
680 99-104 (Ocean Drilling Program, 1995).
- 681 49 Stoll, H. M. Limited range of interspecific vital effects in coccolith stable  
682 isotopic records during the Paleocene-Eocene thermal maximum.  
683 *Paleoceanography* **20**, PA1007 (2005).
- 684 50 Dumitrescu, M. & Brassell, S. C. Compositional and isotopic characteristics of  
685 organic matter for the early Aptian Oceanic Anoxic Event at Shatsky Rise,  
686 ODP Leg 198. *Palaeogeogr., Palaeoclimatol., Palaeoecol.* **235**, 168-191  
687 (2006).
- 688 51 Grantham, P. J. & Wakefield, L. L. Variations in the sterane carbon number  
689 distributions of marine source rock derived crude oils through geological time.  
690 *Org. Geochem.* **12**, 61-73 (1988).
- 691 52 Schwark, L. & Empt, P. Sterane biomarkers as indicators of palaeozoic algal  
692 evolution and extinction events. *Palaeogeogr., Palaeoclimatol., Palaeoecol.*  
693 **240**, 225-236 (2006).
- 694 53 Volkman, J. Sterols in microorganisms. *Appl Microbiol Biotechnol* **60**, 495-  
695 506 (2003).
- 696 54 Brassell, S. C. & Dumitrescu, M. Recognition of alkenones in a lower Aptian  
697 porcellanite from the west-central Pacific. *Org. Geochem.* **35**, 181-188 (2004).
- 698 55 Dumitrescu, M. & Brassell, S. C. Biogeochemical assessment of sources of  
699 organic matter and paleoproductivity during the early Aptian Oceanic Anoxic  
700 Event at Shatsky Rise, ODP Leg 198. *Org. Geochem.* **36**, 1002-1022 (2005).
- 701 56 Bottini, C. *et al.* Climate variability and ocean fertility during the Aptian Stage.  
702 *Clim. Past* **11**, 383-402 (2015).
- 703 57 Andersen, N., Müller, P. J., Kirst, G. & Schneider, R. R. in *Use of Proxies in*  
704 *Paleoceanography* (eds Gerhard Fischer & Gerold Wefer) Ch. 19, 469-488  
705 (Springer Berlin Heidelberg, 1999).

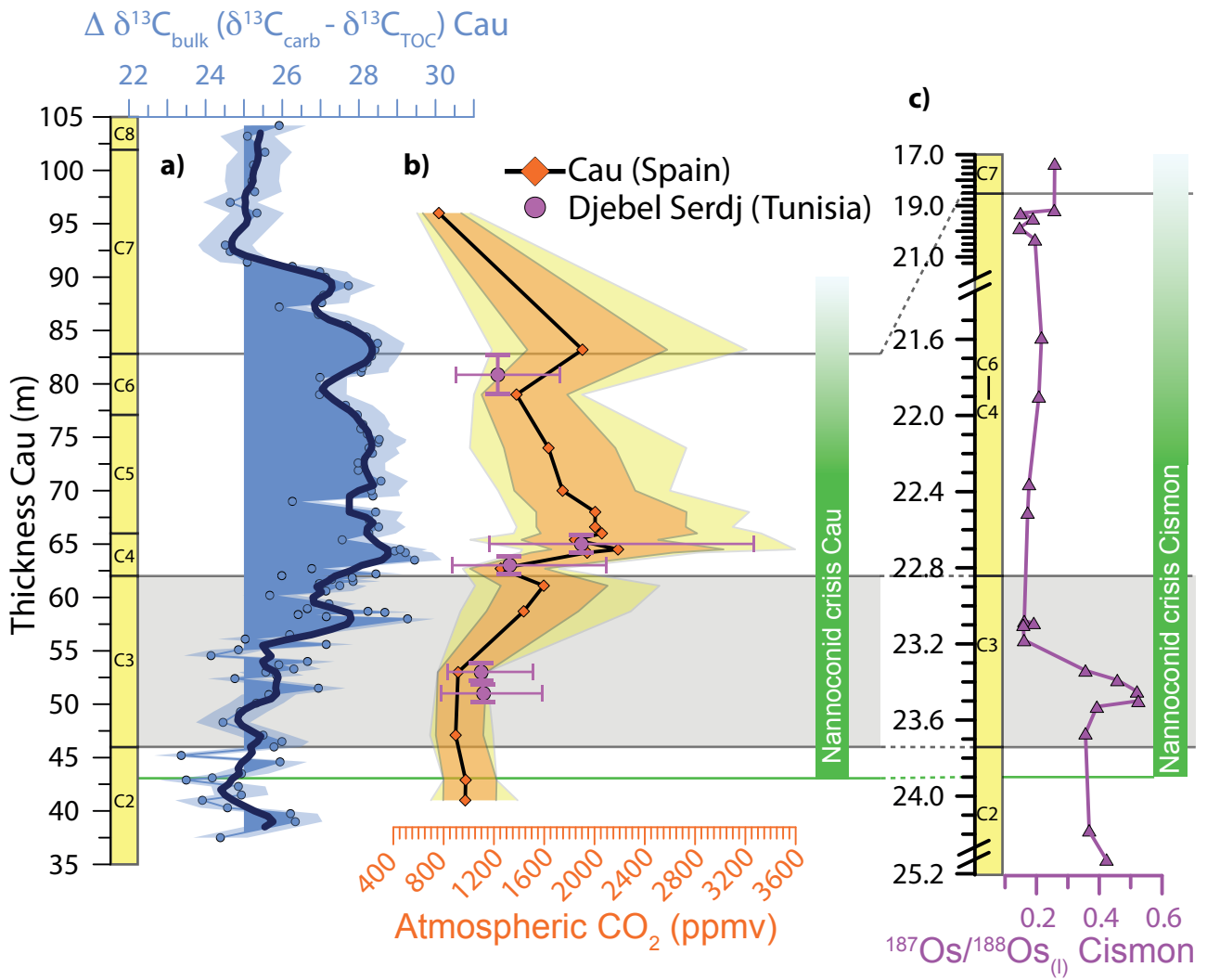
- 706 58 Schulte, S., Benthien, A., Andersen, N., Müller, P. J. & Schneider, R. in *The*  
707 *South Atlantic in the Late Quaternary: Reconstruction of Material Budget and*  
708 *Current Systems* (eds G. Wefer, S. Mulitza, & V. Ratmeyer) 195-211  
709 (Springer, 2003).
- 710 59 Pagani, M. The Alkenone-CO<sub>2</sub> Proxy and Ancient Atmospheric Carbon  
711 Dioxide. *Philos. T. Roy. Soc. A.* **360**, 609-632 (2002).
- 712 60 Kuypers, M. M. M., van Breugel, Y., Schouten, S., Erba, E. &  
713 Sinninghe Damsté, J. S. N<sub>2</sub>-fixing cyanobacteria supplied nutrient N for  
714 Cretaceous oceanic anoxic events. *Geology* **32**, 853-856 (2004).
- 715 61 Pancost, R. D. *et al.* Reconstructing Late Ordovician carbon cycle variations.  
716 *Geochim. Cosmochim. Ac.* **105**, 433-454 (2013).
- 717 62 Schouten, S., Hopmans, E. C., Schefuss, E. & Sinninghe Damsté, J. S.  
718 Distributional variations in marine crenarchaeotal membrane lipids: a new tool  
719 for reconstructing ancient sea water temperatures? *Earth Plant. Sc. Lett.* **204**,  
720 265-274 (2002).
- 721 63 Schouten, S. *et al.* Extremely high sea-surface temperatures at low latitudes  
722 during the middle Cretaceous as revealed by archaeal membrane lipids.  
723 *Geology* **31**, 1069-1072 (2003).
- 724 64 Schouten, S., Hopmans, E. C. & Sinninghe Damsté, J. S. The effect of  
725 maturity and depositional redox conditions on archaeal tetraether lipid  
726 palaeothermometry. *Org. Geochem.* **35**, 567-571 (2004).
- 727 65 Schouten, S., Hopmans, E. C. & Sinninghe Damsté, J. S. The organic  
728 geochemistry of glycerol dialkyl glycerol tetraether lipids: A review. *Org.*  
729 *Geochem.* **54**, 19-61 (2013).
- 730 66 Kim, J.-H. *et al.* New indices and calibrations derived from the distribution of  
731 crenarchaeal isoprenoid tetraether lipids: Implications for past sea surface  
732 temperature reconstructions. *Geochim. Cosmochim. Ac.* **74**, 4639-4654 (2010).
- 733 67 Littler, K., Robinson, S. A., Bown, P. R., Nederbragt, A. J. & Pancost, R. D.  
734 High sea-surface temperatures during the Early Cretaceous Epoch. *Nature*  
735 *Geosci.* **4**, 169-172 (2011).
- 736 68 Jenkyns, H. C., Forster, A., Schouten, S. & Sinninghe Damsté, J. S. High  
737 temperatures in the Late Cretaceous Arctic Ocean. *Nature* **432**, 888-892  
738 (2004).
- 739 69 Jenkyns, H. C., Schouten-Huibers, L., Schouten, S. & Sinninghe Damsté, J. S.  
740 Warm Middle Jurassic-Early Cretaceous high-latitude sea-surface  
741 temperatures from the Southern Ocean. *Clim. Past* **8**, 215-226 (2012).
- 742 70 Tarduno, J. A. *et al.* Evidence for Extreme Climatic Warmth from Late  
743 Cretaceous Arctic Vertebrates. *Science* **282**, 2241-2243 (1998).
- 744 71 Dumitrescu, M., Brassell, S. C., Schouten, S., Hopmans, E. C. &  
745 Sinninghe Damsté, J. S. Instability in tropical Pacific sea-surface temperatures  
746 during the early Aptian. *Geology* **34**, 833-836 (2006).
- 747 72 Hopmans, E. C. *et al.* A novel proxy for terrestrial organic matter in sediments  
748 based on branched and isoprenoid tetraether lipids. *Earth Plant. Sc. Lett.* **224**,  
749 107-116 (2004).
- 750 73 Pearson, P. N. *et al.* Stable warm tropical climate through the Eocene Epoch.  
751 *Geology* **35**, 211-214 (2007).
- 752 74 Hu, X., Zhao, K., Yilmaz, I. O. & Li, Y. Stratigraphic transition and  
753 palaeoenvironmental changes from the Aptian oceanic anoxic event 1a  
754 (OAE1a) to the oceanic red bed 1 (ORB1) in the Yenicesihlar section, central  
755 Turkey. *Cretaceous Res.* **38**, 40-51 (2012).

756 75 Huck, S., Heimhofer, U., Rameil, N., Bodin, S. & Immenhauser, A. Strontium  
757 and carbon-isotope chronostratigraphy of Barremian–Aptian shoal-water  
758 carbonates: Northern Tethyan platform drowning predates OAE 1a. *Earth*  
759 *Plant. Sc. Lett.* **304**, 547-558 (2011).  
760  
761







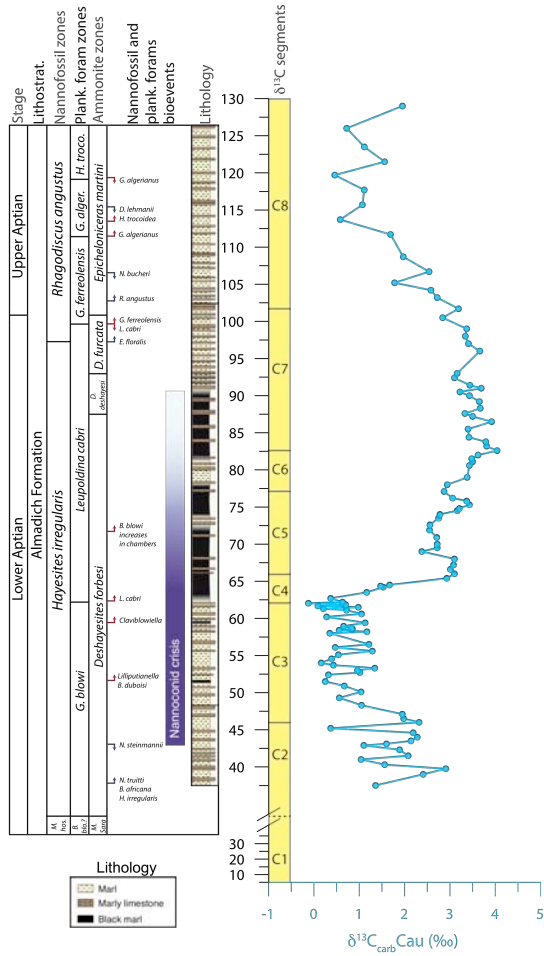


# Gradual and sustained carbon dioxide release during Aptian Oceanic Anoxic Event 1a

## Event 1a

### Supplementary figures

#### Cau, S. Spain



#### Bedoule outcrops, S.E. France

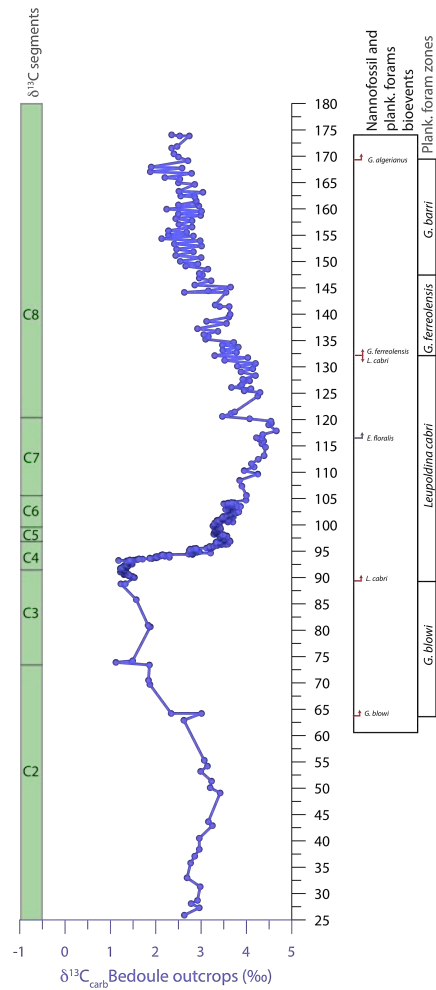


**Figure S1: Comparison of  $\delta^{13}\text{C}_{\text{carb}}$  records 1**

$\delta^{13}\text{C}_{\text{carb}}$  data from Cau (left) and SE France (right)<sup>S1</sup> on their individual depth scales and published biostratigraphy.

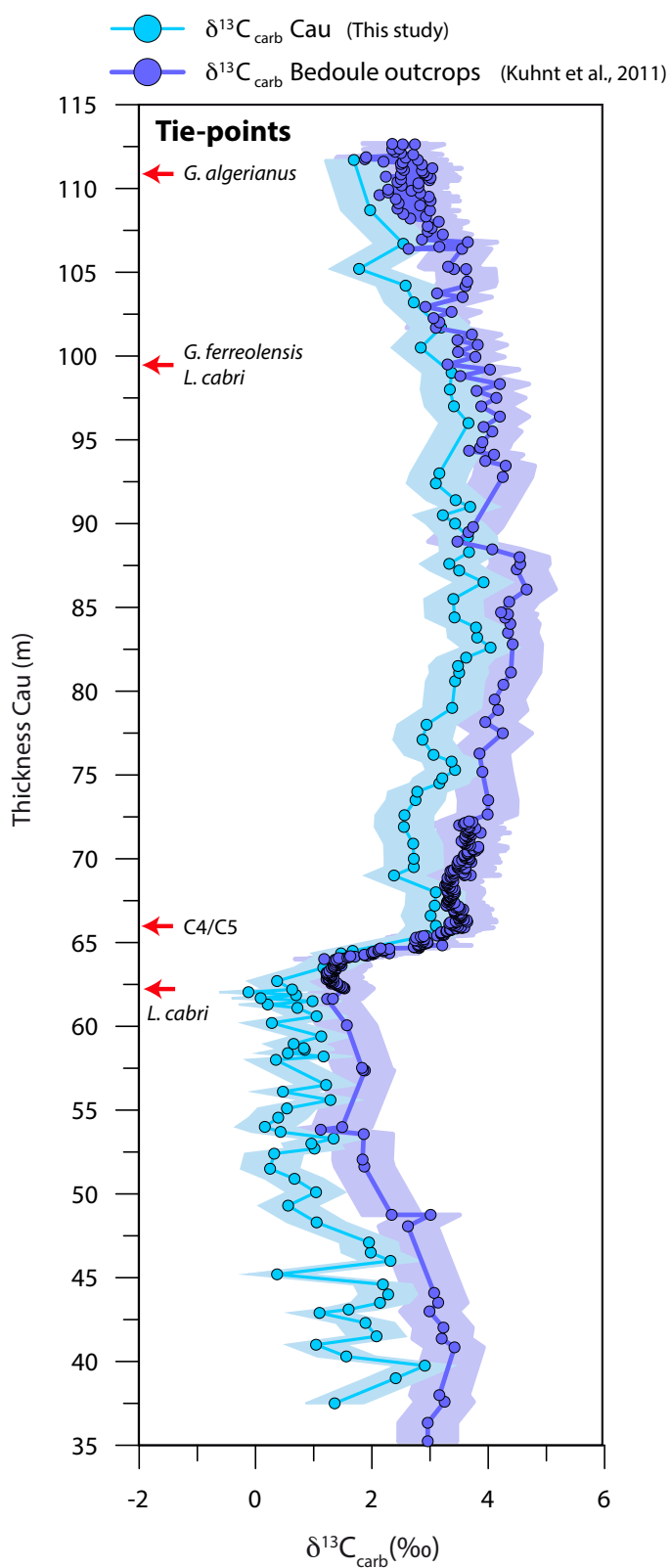


**Figure S2: Comparison of  $\delta^{13}\text{C}_{\text{carb}}$  records 2**

$\delta^{13}\text{C}_{\text{carb}}$  data from SE France<sup>SI</sup> tuned to Cau using a minimal of four tie-points (indicated by red arrows) to demonstrate the similarity in structure and magnitude of change. Shaded areas represent 0.5 ‰ uncertainty.

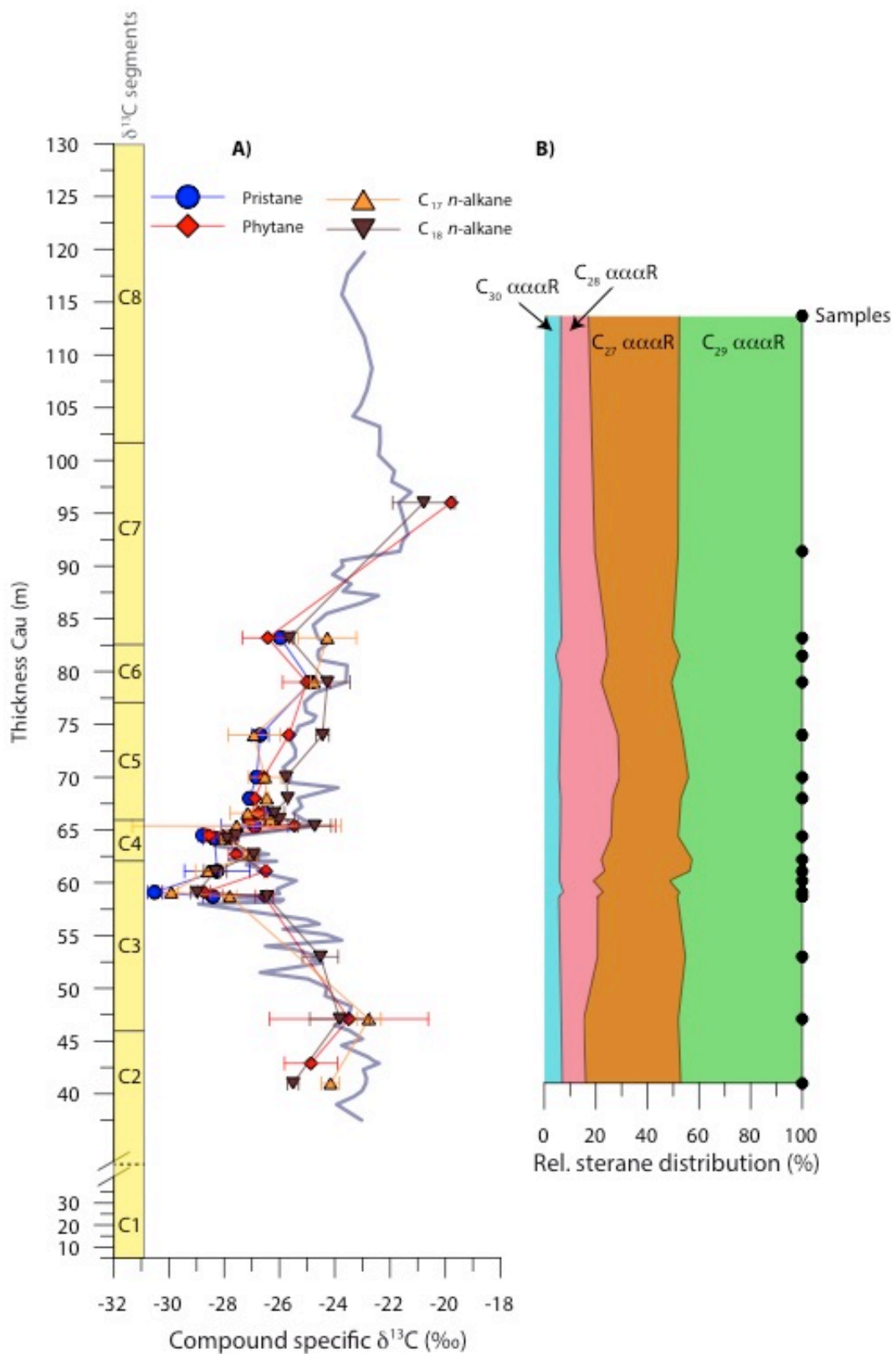


**Figure S3: Sterane distribution at Cau**

a)  $\delta^{13}\text{C}_{\text{TOC}}$  and  $\delta^{13}\text{C}_{\text{alg}}$  across OAE 1a at Cau together with b) relative  $\text{C}_{27}$ - $\text{C}_{30}$  αααR sterane distribution.

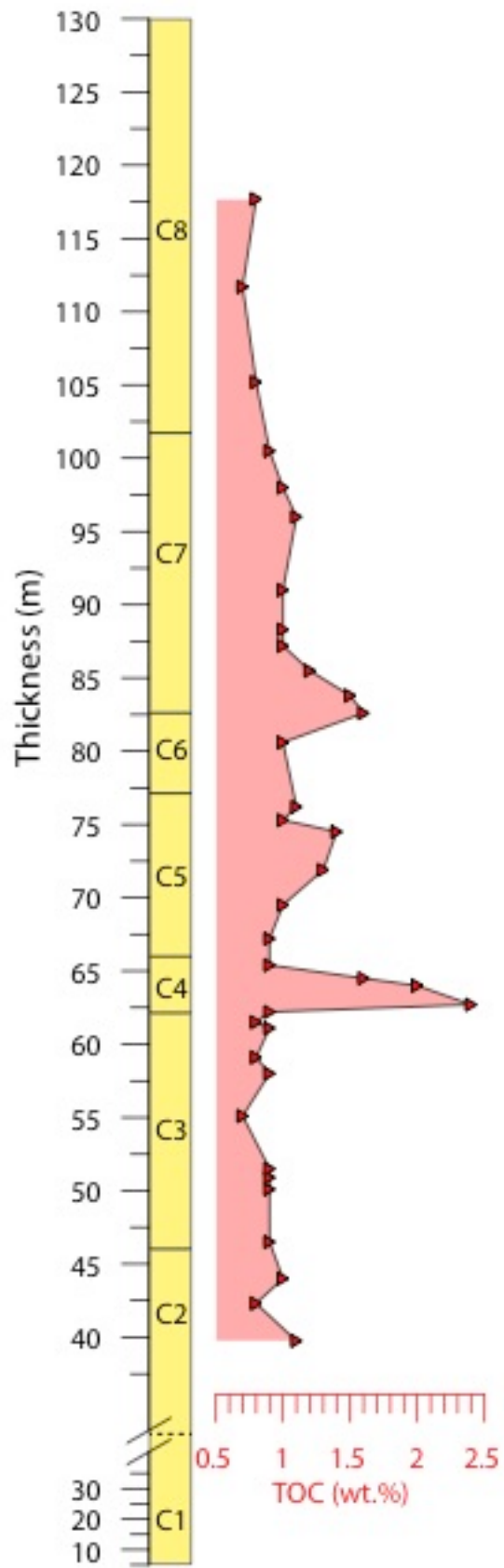
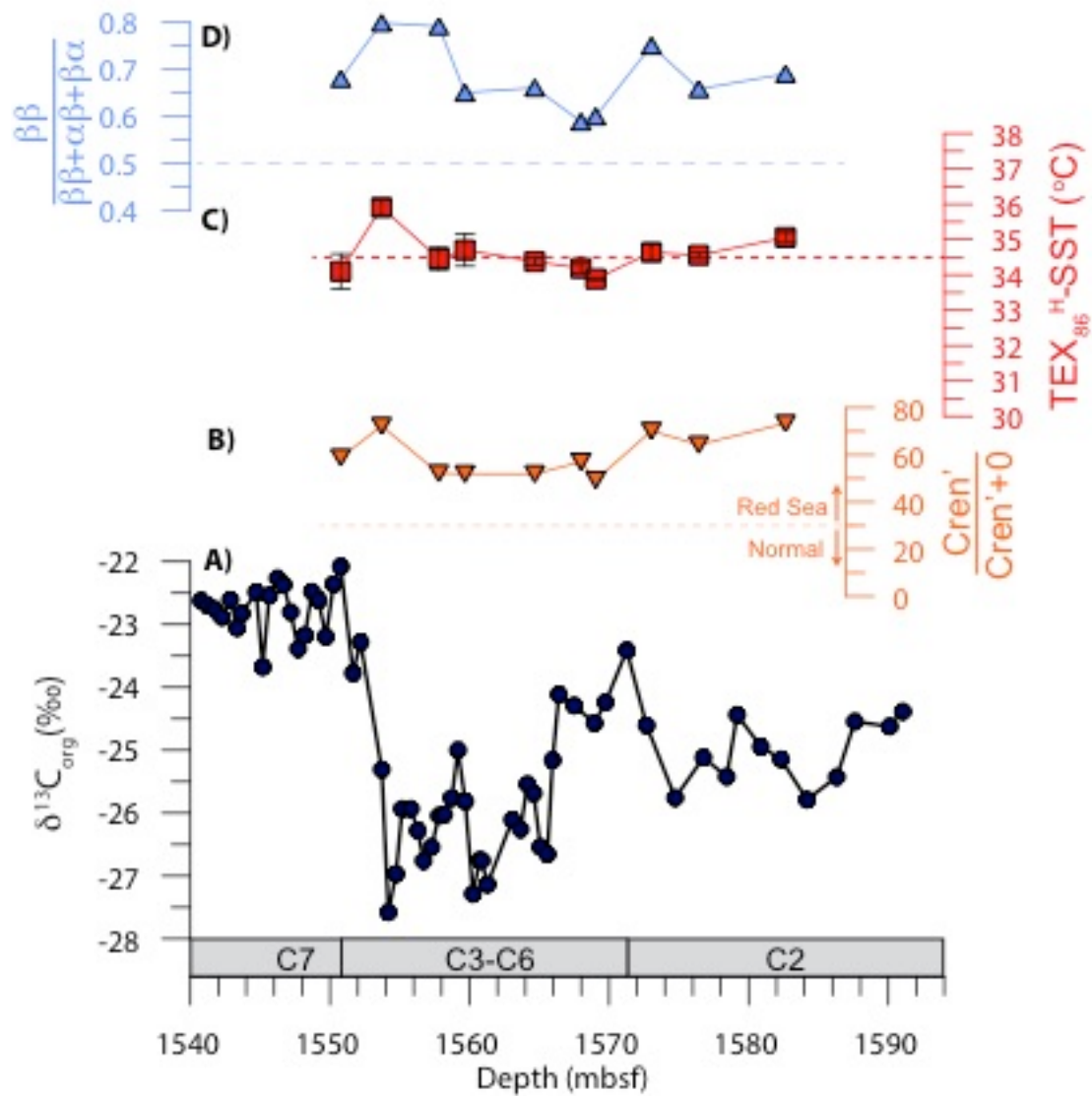
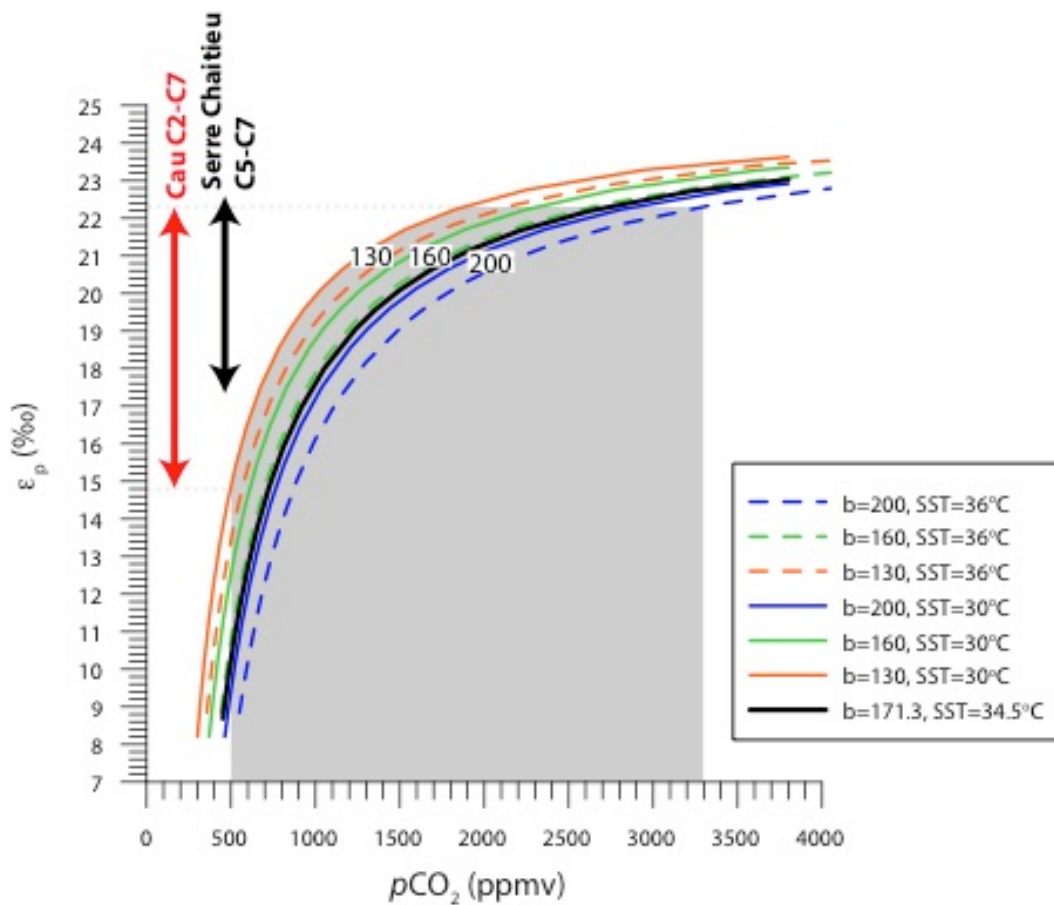


Figure S4; Total organic carbon (TOC) record from Cau.



**Figure S5; Sea surface temperatures across OAE 1a**

a) bulk  $\delta^{13}\text{C}_{\text{org}}$  across OAE 1a at DSDP Site 398 with C-isotope stratigraphy<sup>S2</sup> together with b) ratio of crenarchaeol abundance over GDGT-0, c) SSTs, based on the  $\text{TEX}_{86}^{\text{H}}$ -calibration<sup>S3</sup>, and d)  $\text{C}_{31}$  hopane maturity index. Error bars on  $\text{TEX}_{86}^{\text{H}}$ -SSTs represent  $1\sigma$  of duplicates.



**Figure S6; Relationship between  $\epsilon_p$  and  $pCO_2$**

The relationship between  $\epsilon_p$  and  $pCO_2$ , assuming SSTs values between 30 (continuous lines) and 36 °C (dashed lines) and  $b$  values of 130 (orange), 160 (green), and 200 (blue). For our  $pCO_2$  calculations we assumed a constant SST of 34.5 °C and  $b$  value of 171.3 (thick black line). The range of  $\epsilon_p$  values observed across segments C2 to C7 at Cau (red arrow) and segment C5 to C7 at Serre Chaitieu<sup>S4</sup> (black arrow) are also indicated.

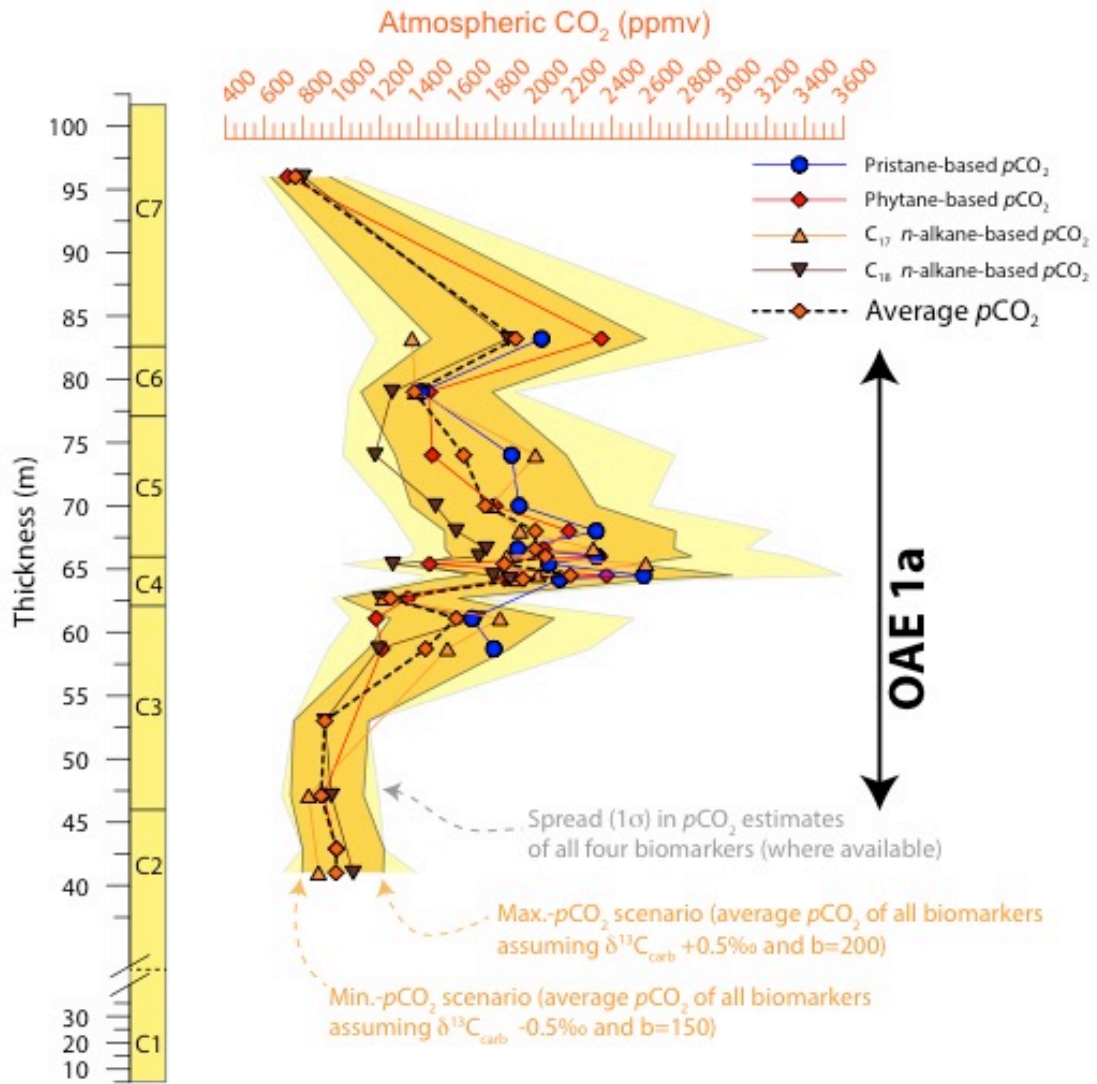


**Figure S7; Uncertainty envelopes**  
 $p\text{CO}_2$  estimates derived from the  $\delta^{13}\text{C}$  values of individual biomarkers, as well as the resulting average that is used in Figure 3 of the main manuscript.



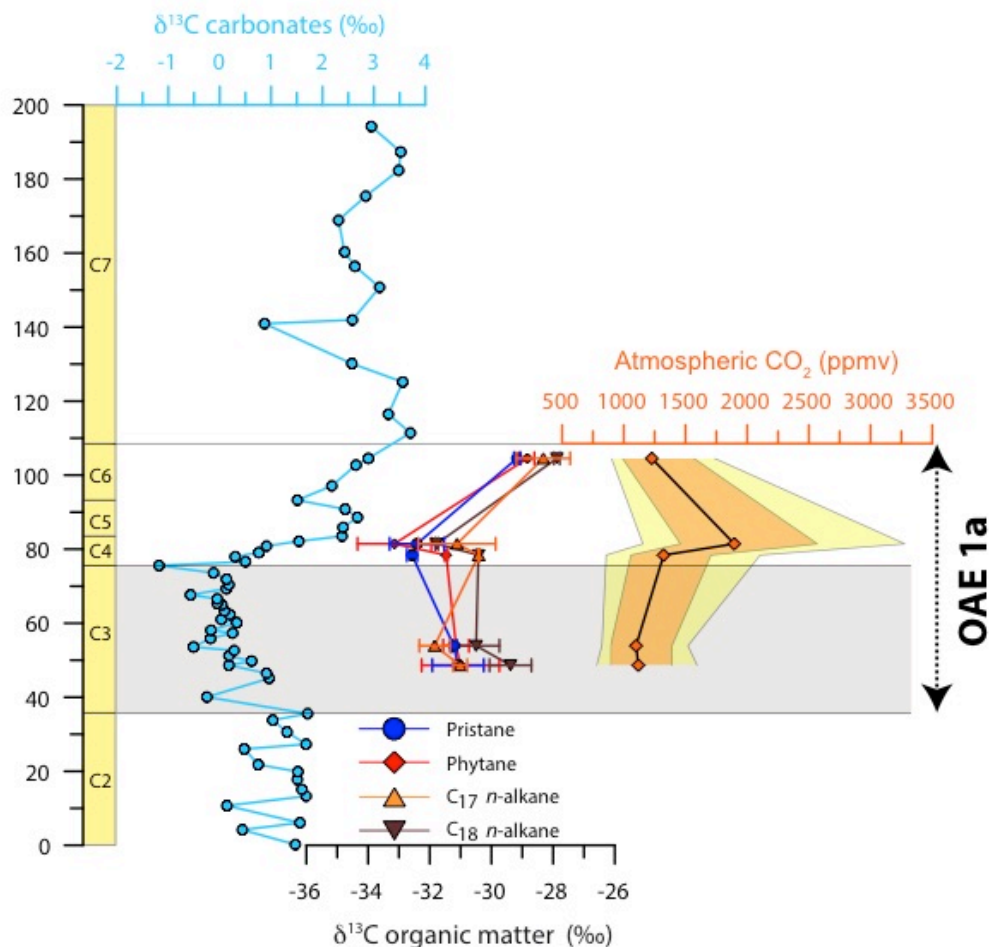


**Figure S8;  $\delta^{13}\text{C}$  and  $p\text{CO}_2$  Djebel Serdj formation in Tunisia**

$\delta^{13}\text{C}_{\text{carb}}^{\text{S5}}$  together with low-resolution  $\delta^{13}\text{C}_{\text{alg}}$  (not corrected to bulk biomass) and  $p\text{CO}_2$  record, calculated using the exact same assumption as used to calculate  $p\text{CO}_2$  at Cau.

#### Supplementary References

- S1 Kuhnt, W., Holbourn, A. & Moullade, M. Transient global cooling at the onset of early Aptian oceanic anoxic event (OAE) 1a. *Geology* **39**, 323-326 (2011).
- S2 Li, Y.-X. *et al.* Toward an orbital chronology for the early Aptian Oceanic Anoxic Event (OAE1a, ~ 120 Ma). *Earth Plant. Sc. Lett.* **271**, 88-100 (2008).
- S3 Kim, J.-H. *et al.* New indices and calibrations derived from the distribution of crenarchaeal isoprenoid tetraether lipids: Implications for past sea surface temperature reconstructions. *Geochim. Cosmochim. Ac.* **74**, 4639-4654 (2010).
- S4 Heimhofer, U., Hochuli, P. A., Herrle, J. O., Andersen, N. & Weissert, H. Absence of major vegetation and palaeoatmospheric  $p\text{CO}_2$  changes associated with oceanic anoxic event 1a (Early Aptian, SE France). *Earth Plant. Sc. Lett.* **223**, 303-318 (2004).
- S5 Heldt, M., Bachmann, M. & Lehmann, J. Microfacies, biostratigraphy, and geochemistry of the hemipelagic Barremian–Aptian in north-central Tunisia: Influence of the OAE 1a on the southern Tethys margin. *Palaeogeogr., Palaeoclimatol., Palaeoecol.* **261**, 246-260 (2008).